Link to Editor. DOI: 10.1016/j.ejmech.2020.112395

Privileged Scaffold-Based Design to Identify a Novel Drug-like 5-HT$_7$ Receptor-Preferring Agonist to Target Fragile X Syndrome

Enza Lacivita,[a] Mauro Niso,[a] Madia Letizia Stama,[a] Anna Arzuaga,[b] Concetta Altamura,[c] Lara Costa,[d] Jean-François Desaphy,[c] Michael E. Ragozzino,[e] Lucia Ciranna,[f] Marcello Leopoldo[a]*

[a]Dipartimento di Farmacia-Scienze del Farmaco, Università degli Studi di Bari Aldo Moro, via Orabona 4, 70125 Bari, Italy

[b]Department of Biological Sciences, University of Illinois at Chicago, Chicago, IL 60607, USA

[c]Department of Biomedical Sciences and Human Oncology, Università degli Studi di Bari Aldo Moro, Policlinico, piazza Giulio Cesare, 70126 Bari, Italy

[d]Dipartimento di Medicina Clinica e Sperimentale, Università di Messina, Via Consolare Valeria 1, Messina, Italy

[e]Department of Psychology, University of Illinois at Chicago, Chicago, IL 60607, USA

[f]Dipartimento di Scienze Biomediche e Biotecnologiche, Università di Catania, Via Santa Sofia 97, Catania, Italy

*Corresponding Author: Marcello Leopoldo, Dipartimento di Farmacia – Scienze del Farmaco, Università degli Studi di Bari Aldo Moro, via Orabona, 4, 70125, Bari, Italy. E-mail: marcello.leopoldo@uniba.it. Phone: +39 080 5442798. Fax: +39 080 5442231.

ABSTRACT

Recent preclinical studies have shown that activation of the serotonin 5-HT_7 receptor has the potential to treat neurodevelopmental disorders such as Fragile X syndrome, a rare disease characterized by autistic features. With the aim to provide the scientific community with diversified drug-like 5-HT_7 receptor-preferring agonists, we designed a set of new long-chain arylpiperazines by exploiting structural fragments present in clinically approved drugs or in preclinical candidates (privileged scaffolds). The new compounds were synthesized, tested for their affinity at 5-HT_7 and 5-HT_{1A} receptors, and screened for their in vitro stability to microsomal degradation and toxicity. Selected compounds were characterized as 5-HT_7 receptor-preferring ligands, endowed with high metabolic stability and low toxicity. Compound **7g** emerged as a drug-like 5-HT_7 receptor-preferring agonist capable to rescue synaptic plasticity and attenuate stereotyped behavior in a mouse model of Fragile X syndrome.

HIGHLIGHTS

- 5-HT_7 receptor agonists have the potential to treat Fragile X syndrome
- 21 drug-like 5-HT_7 receptor ligands were synthesized by exploiting privileged scaffolds
- **7g** displayed good pharmacokinetic properties and low in vitro toxicity
- **7g** is a 5-HT_7 receptor-preferring agonist capable to rescue long-term synaptic plasticity
- **7g** attenuates stereotyped behavior in a mouse model of Fragile X syndrome

Graphical Abstract

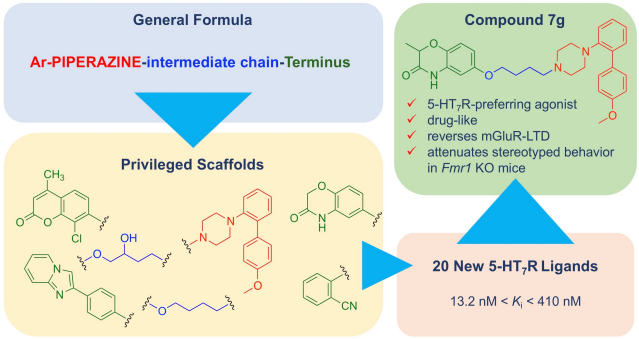

KEYWORDS

5-HT$_7$ receptor, arylpiperazine, Fragile X Syndrome, privileged scaffold-based design, pharmacokinetic properties

ABBREVIATIONS

5-HT$_{1A}$R: serotonin 1A receptor; 5-HT$_7$R: serotonin 7 receptor; AMPA: α-amino-3-hydroxy-5-methyl-4-isoxazolepropionic acid; BBB: blood-brain barrier; cAMP: cyclic adenosine monophosphate; $CL_{int,\ app}$: apparent intrinsic clearance; CNS: central nervous system; CYP: Cytochrome P450; DHPG: (*S*)-3,5-dihydroxyphenylglycine; EPSC: Excitatory post-synaptic current; FDA: Food and Drug Administration; FMR1: Fragile X mental retardation 1; FXS: Fragile X syndrome; f_u: unbound fraction; hERG, ether- a-go-go-related gene; ip: intraperitoneal injection; LTD: long term depression; mGluR: metabotropic glutamate receptor; MTT: 3-(4,5-dimethylthiazol-2-yl)-2,5-diphenyl tetrazolium bromide; SAR: structure-activity relationship

INTRODUCTION

Serotonin receptor type 7 (5-HT$_7$R) is a G-protein coupled receptor, belonging to the family of serotonin receptors. In the mouse brain, the 5-HT$_7$R is distributed in discrete areas such as the hippocampus, hypothalamus, thalamus, hypothalamus, cortex, raphe nuclei, and striatum. A similar distribution has been observed in other mammalian species, including human [1,2]. Several studies have indicated the involvement of the central nervous system (CNS) 5-HT$_7$R in important functional roles such as thermoregulation, circadian rhythm, learning and memory, and sleep [3]. The activation of 5-HT$_7$R results in an intracellular increase of cyclic adenosine monophosphate (cAMP) via a Gs protein or activation of a G12 protein. At the cellular level, activation of 5-HT$_7$R modulates neuronal morphology in hippocampal, striatal, and cortical neuronal cultures from mice and rats [4–7], as well as in primary embryonic cultures from the same species [8,9]. The intracellular signaling pathways downstream to 5-HT$_7$R activation involves the activation of RhoA and Cd42 proteins [5,6,8,9]. These proteins belong to the Rho family GTPase which are key players in neuronal morphology (dendritic arborization, spine morphogenesis, growth cone development, and axon guidance) and connectivity [10]. Over the years, selective 5-HT$_7$R agonists have become available [11], including LP-211 (Figure 1). Activation of 5-HT$_7$R by LP-211 is able to rescue impaired synaptic plasticity in wild type and *Fmr1* KO mice, an animal model of Fragile-X syndrome (FXS), a rare X-linked disease with autistic features, such as mental retardation and stereotyped behavior [12,13]. In particular, activation of 5-HT$_7$R in hippocampal slices from *Fmr1* KO mice was able to rescue abnormalities in metabotropic glutamate receptor-dependent long-term depression (mGluR-LTD) [12], which is abnormally enhanced in the hippocampus of *Fmr1* KO mice [14]. Importantly, a systemic administration of LP-211 to *Fmr1* KO mice corrected learning deficits and repetitive behavior [15]. 5-HT$_7$ R stimulation by LP-211 has been shown to revert neurobehavioral phenotypes in MeCP2 KO mice, a mice model of Rett syndrome, a neurodevelopmental disease characterized by intellectual disability [16,17]. At the cellular level, stimulation of 5-HT$_7$R does impact Rho GTPases-mediated signaling pathways and rescues

mitochondrial respiratory chain impairment, oxidative phosphorylation deficiency, and the reduced energy status in MeCP2 KO mice brain [16,18]. In addition, in a mouse model of CDKL5 Deficiency Disorder, a rare neurodevelopmental syndrome characterized by severe behavioral and physiological symptoms [19], stimulation of 5-HT_7R with LP-211 partially rescues the abnormal phenotype and brain molecular alterations.

Altogether these findings suggest that 5-HT_7R agonists could be of therapeutic relevance in psychiatric disorders characterized by impaired synaptic plasticity such as FXS or Rett syndrome and, possibly, idiopathic autism spectrum disorder [20,21].

Medicinal chemistry efforts have led to the identification of selective 5-HT_7R agonists, such as LP-211, AS-19, and E-55888 (Figure 1). As illustrated above, the brain penetrant selective 5-HT_7R agonist LP-211 has been employed in seminal studies to propose 5-HT_7R as a therapeutic target for FXS and RTT. The search for new 5-HT_7R agonist is still active as witnessed by the recent discovery of the low-basicity highly selective 5-HT_7R agonist AGH-192 (Figure 1) [22]. As part of our continuing efforts to provide the scientific community with diversified 5-HT_7R-preferring agonists suitable for studies in vivo, we have pursued the development of a new 5-HT_7R agonist ideally free from intrinsic liabilities. In a recent paper, Taylor and coworkers suggested that exploiting the known "clinically validated space" before focusing on novel scaffolds might be a pragmatic approach to enrich a screening collection [23]. The authors were referring to focused molecules (or scaffolds or moieties), with a proven pedigree for drug discovery, which would be an extremely useful subset of chemical space for drug discovery. Having this concept in mind, we focused on **1a** (BA-10) (Figure 1, Table 1), a 5-HT_7R agonist [13] that features the aryloxy propanolamine motif as many FDA-approved beta-adrenergic blocking agents, including propranolol (Figure 2). Compound **1a** was indeed identified to possess some drug-like properties, as a positron emission tomography study in vivo in pigs showed that [^{11}C]**1a** was able to pass the blood-brain barrier (BBB) and was not a substrate of efflux systems present on the BBB such as P-glycoprotein [24]. However, the study showed that [^{11}C]**1a** underwent metabolic degradation *in*

vivo, with 40% of the compound remaining after 10 min. Thus, we manipulated the scaffold of **1a** targeting compounds with improved drug-like properties while maintaining favorable 5-HT$_7$R potency and selectivity. This strategy succeeded in the identification of a new 5-HT$_7$R-preferring agonist suitable for studies in vivo.

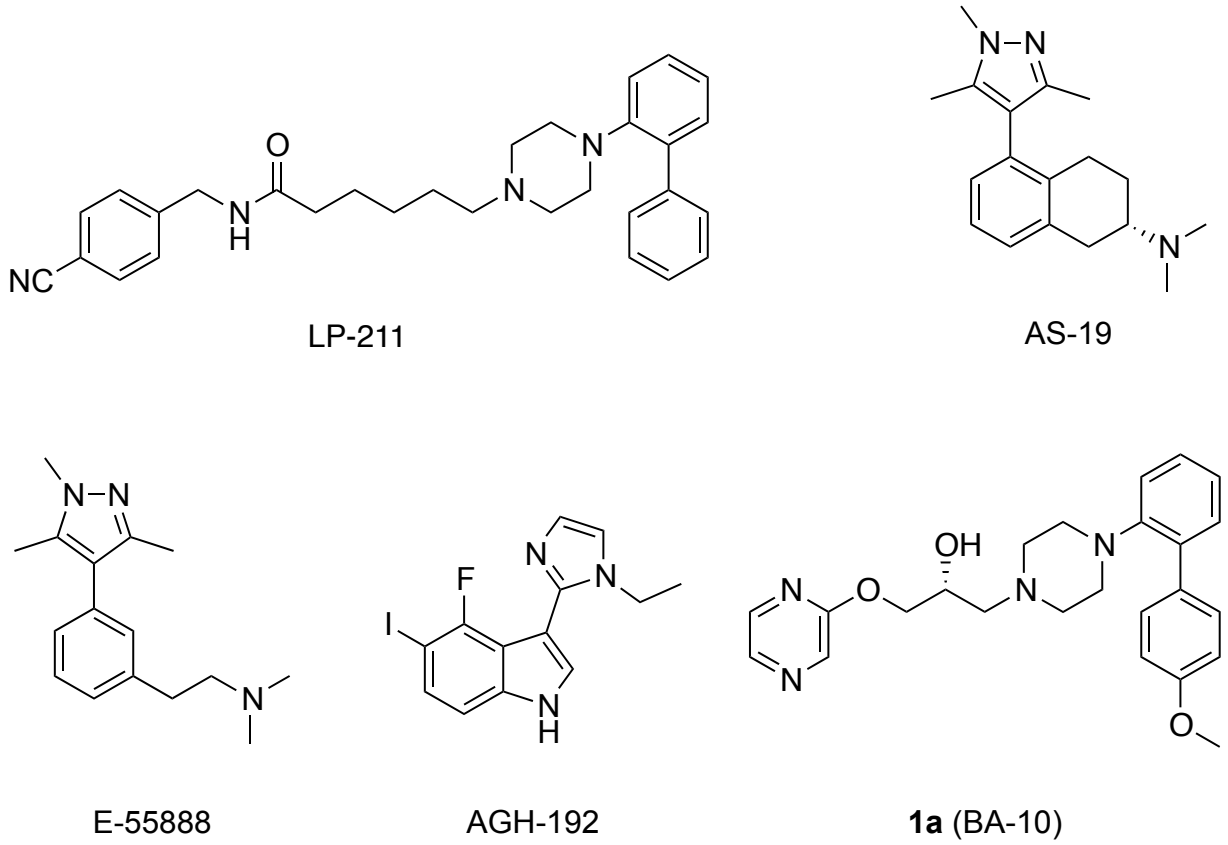

Figure 1. Structural Formula of Reference 5-HT$_7$ Receptor Agonists

STUDY DESIGN

Compound **1a** belongs to the class of long-chain arylpiperazine which general structure is given by Ar-PIPERAZINE-intermediate chain-Terminus [25]. The design strategy of the new compounds exploited "privileged moieties" (as defined above) that would be compatible with either the structural requirements for high affinity at 5-HT$_7$R and stability towards oxidative metabolism. The aromatic system (Ar) linked to the piperazine ring is a key structural element for 5-HT$_7$R affinity and selectivity. Compound **1a** features a 2-(4-methoxyphenyl)phenyl group which is responsible for high 5-HT$_7$R affinity and selectivity and is more stable to oxidative metabolism than the

corresponding unsubstituted biphenyl compounds [24, 26–28]. Consequently, the 1-[2-(4-methoxyphenyl)phenyl]piperazine structure was selected as privileged basic moiety to design the new 5-HT_7R ligands (Tables 1, 2, and 3). The second structural element of the general formula of the target compounds is the piperazine ring. A previous study showed that the replacement of piperazine with piperidine can lead to an increase of metabolic stability with a loss of 5-HT_7R affinity [28]. Thus, a small group of 4-[2-(4-methoxyphenyl)phenyl]piperidine derivatives were investigated (compounds **14a,e**,**15a,e** Table 3).

The third structural element of the general formula of the target compounds is the intermediate chain. Compound **1a** features the 2-hydroxypropyloxy chain which is present in numerous marketed beta-adrenergic blocking drugs. Consequently, the new compounds **1b–g** (Table 1) featured such privileged moiety. Another structural motif used for this study is the butyloxy intermediate chain which is displayed by the metabolically stable antipsychotic drug aripiprazole [29] (Figure 2) (compounds **7a–g**, Table 2). In addition, three alternative intermediate chains were explored in order to find structural determinants to improve metabolic stability (Table 3, compounds **9**, **25**, and **26**). The fourth structural element of the general formula of the target compounds is the terminus. Previous SAR studies indicated no particular restrictions for the structure of the terminal fragment, as both mono- and bicyclic systems are tolerated with respect to 5-HT_7R affinity. Thus, we searched for mono- and bicyclic systems with a proven pedigree for drug discovery. We selected 4-chloro-3-fluorophenyl- and 4-chloro-2-fluorophenyl- because fluorinated derivatives are often specifically designed to increase metabolic stability over the hydrogen-substituted counterparts (compounds **1b,c** in Table 1 and compounds **7b,c** in Table 2) [30]. Next, we selected the imidazo[1,2-*a*]pyridine system to design compounds **1e** (Table 1), **7e** (Table 2), **14e** and **15e** (Table 3) because from the screening of the in-house library of arylpiperazine-based compounds we identified the derivative **2** (Figure 2) [31], as endowed with stability toward oxidative metabolism (36% of recovery after 30 min incubation with rat microsomes). Another privileged moiety was the decorated coumarin system which is present in the metabolically stable investigational compound **3** (Figure 2) [32].

Finally, terminal fragments inspired by the FDA-approved drugs bunitrol or brilaroxazine [33] (Figure 2) were exploited in the case of compounds **1d,g** (Table 1) and **7d,g** (Table 2).

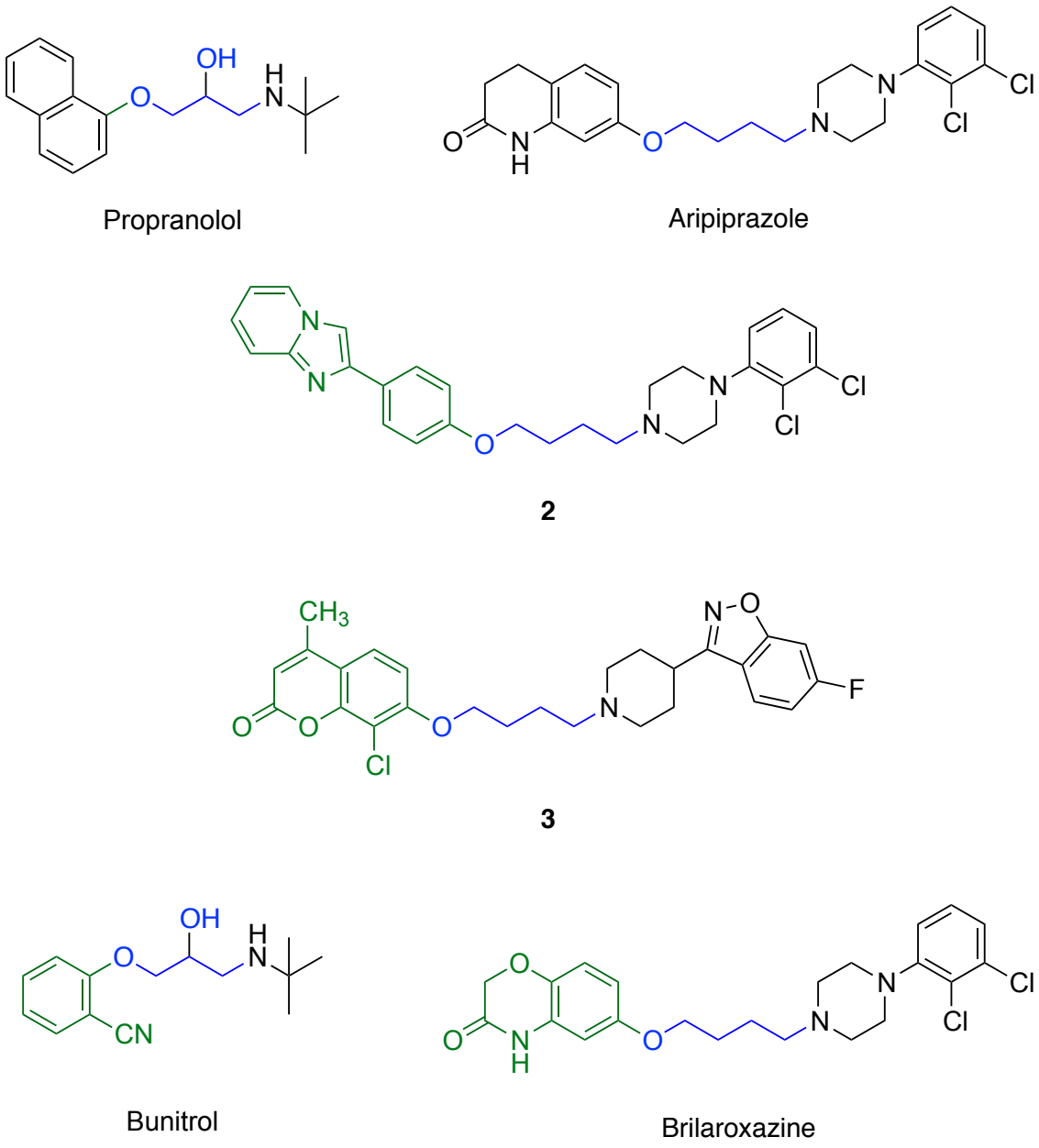

Figure 2. Structural Formula of Reference Compounds

CHEMISTRY

The synthesis of the final compounds bearing the 2-hydroxypropyloxy spacer was accomplished by reacting the appropriate phenol **4b–g** with (*R*)-glycidylnosilate to afford the intermediate epoxides

5b–g which were condensed with 1-[2-(4-methoxyphenyl)phenyl]piperazine to give the target compounds **1b–g** (Scheme 1).

The final compounds featuring a butyloxy intermediate chain were synthesized by reacting the appropriate phenol with 1-bromo-4-chlorobutane to give 4-chlorobutyl derivatives **6b–g**, which were reacted with 1-[2-(4-methoxyphenyl)phenyl]piperazine to give the target compounds **7b–g** (Scheme 1).

Compound **9** was prepared by starting from 4-chloro-3-fluorophenol (**4b**) which reacted with 1-chloro-4-bromo-2-butyne to give the intermediate **8**, which was condensed with 1-[2-(4-methoxyphenyl)phenyl]piperazine to afford the target compound (Scheme 1).

The target compounds containing the piperidine ring were synthesized according to Scheme 2. 2-(4-Methoxyphenyl)benzaldehyde (**10**) was condensed with diethyl acetoacetate in the presence of piperidine and then hydrolyzed under acidic conditions to give diacid **11**. This latter was reacted with urea to give the imide **12** which was reduced with $LiAlH_4$ to afford piperidine **13**. This amine was then alkylated with intermediates **5a**,**e** to give the final compounds **14a,e** or with intermediates **22** and **6e** to give the final compounds **15a,e**.

The compounds featuring the terminal pyrazine ring were prepared as depicted in Scheme 3. 2-Chloropyrazine was reacted with diols **16–18** to give the alcoholic intermediates **19–21** which were transformed into the corresponding mesylates **22–24**. These latter were reacted with 1-[2-(4-methoxyphenyl)phenyl]piperazine to give the target compounds **7a**, **25**, and **26**.

Scheme 1.[a]

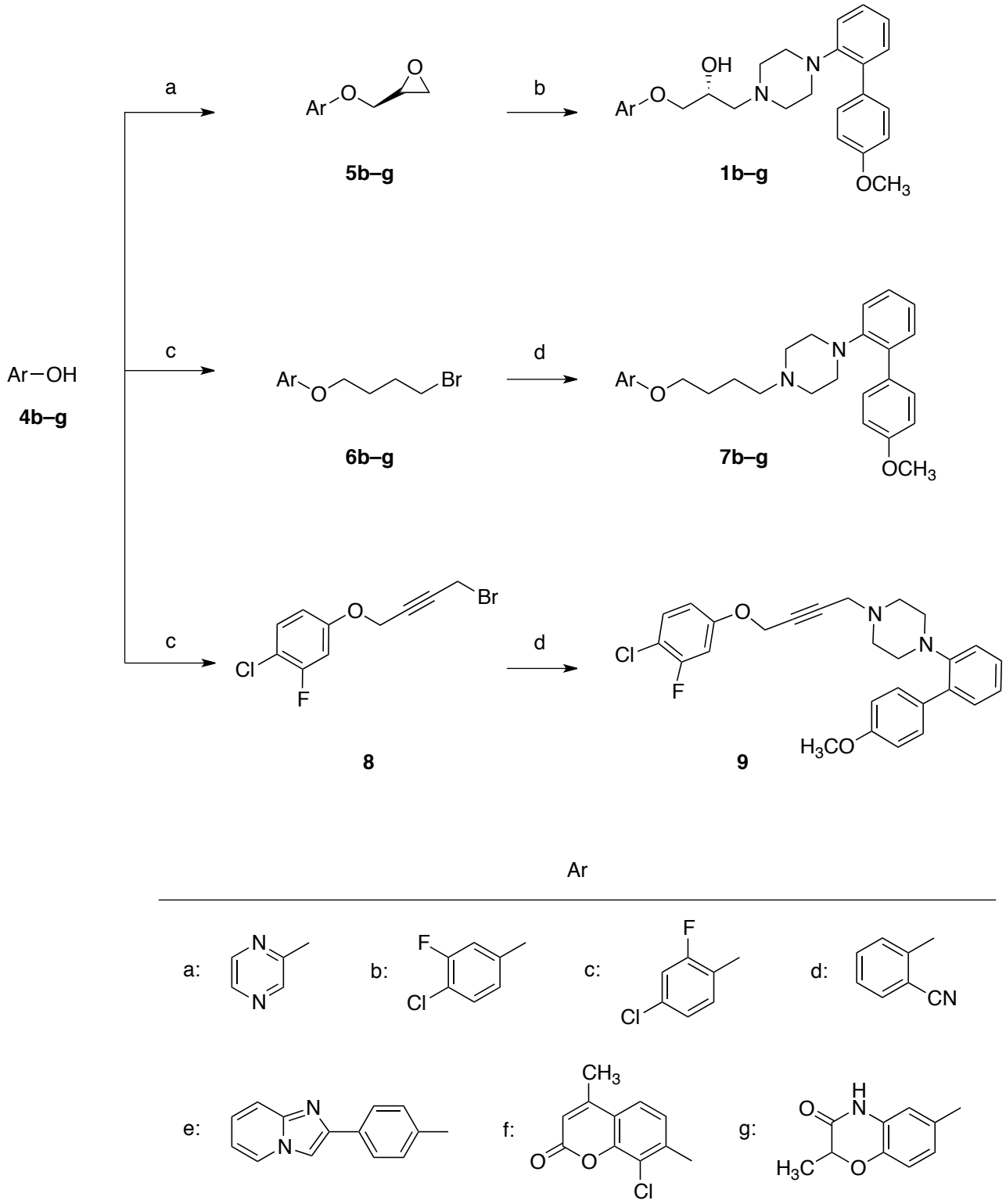

[a]*Reagents and Conditions*: a) (*R*)-glycidyl nosilate, NaH, anhydrous DMF, from 0 °C to r.t., overnight, 41-86% yield; b) 1-[2-(4-methoxyphenyl)phenyl]piperazine or piperidine **13**, EtOH, reflux, 5 h, 30-80% yield; c) 1,4-dibromobutane or 1-chloro-4-bromo-2-butyne, K_2CO_3, acetone, reflux, 5-8 h, from 42% to quantitative yield; d) 1-[2-(4-methoxyphenyl)phenyl]piperazine or piperidine **13**, K_2CO_3, CH_3CN, reflux, overnight, 20-65% yield.

Scheme 2.[a]

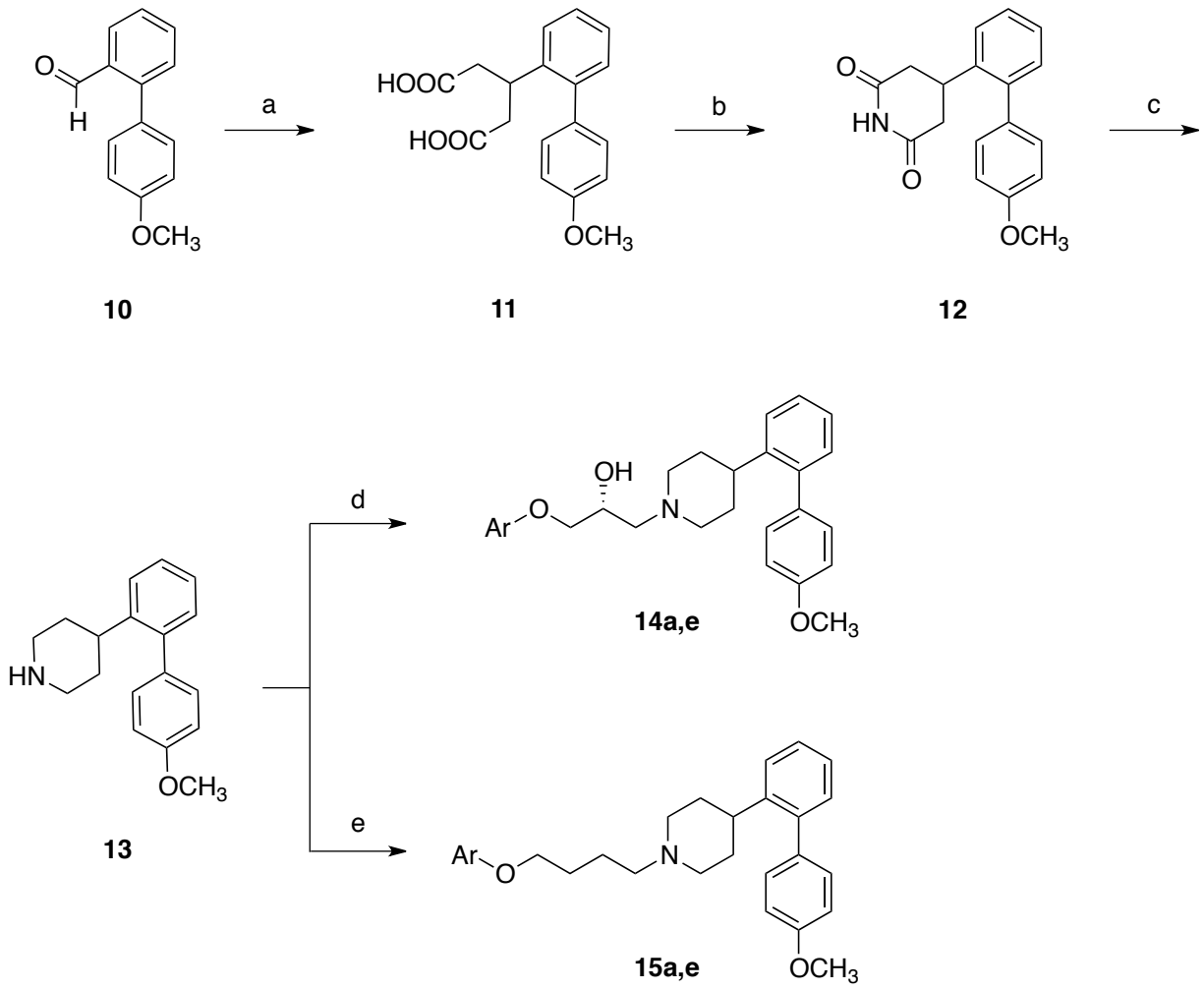

[a]*Reagents and Conditions*: a) i: ethyl acetoacetate, piperidine, EtOH, r.t. 15 h; ii: 12 M NaOH, EtOH, reflux, 4 h, 29% yield; b) urea, 160-165 °C, 2h, 72% yield; c) $LiAlH_4$, anhydrous THF, from 0 °C reflux, 3 h, quantitative yield; d) 1-[2-(4-methoxyphenyl)phenyl]piperazine or piperidine **13**, EtOH, reflux, 5 h, 38-60% yield; e) 1-[2-(4-methoxyphenyl)phenyl]piperazine or piperidine **13**, K_2CO_3, CH_3CN, reflux, overnight, 20-30% yield.

Scheme 3. [a]

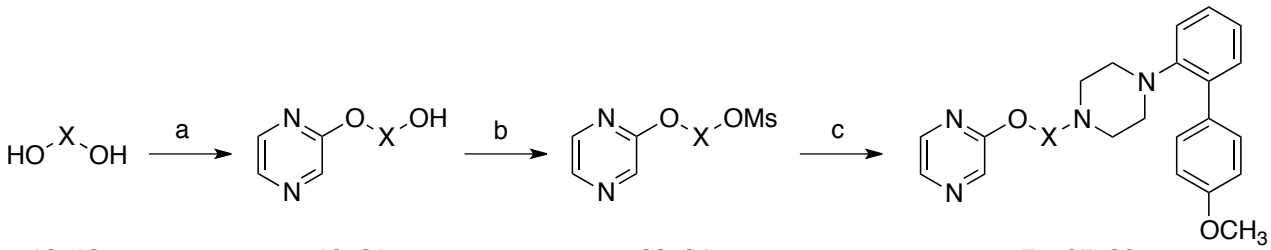

16–18 **19–21** **22–24** **7a**, **25**, **26**

compounds	X
16, **19**, **22, 7a**	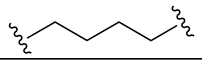
17, **20**, **23, 25**	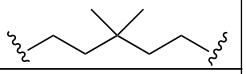
18, 21, 24, 26	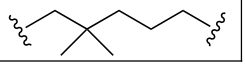

[a]*Reagents and Conditions*: a) 2-chloropyrazine, NaH, anhydrous DMF, from 0 °C to r.t, overnight; 23-40% yield; b) methanesulfonyl chloride, Et_3N, from -10 °C to r.t.; from 40% to quantitative yield; c) 1-[2-(4-methoxyphenyl)phenyl]piperazine, K_2CO_3, CH_3CN, reflux, overnight, 20-39% yield.

RESULTS AND DISCUSSION

Binding affinities to 5-HT$_7$ and 5-HT$_{1A}$ receptors.

All the synthesized compounds were tested in radioligand binding assays to determine their affinity for the target 5-HT$_7$R. In addition, the target compounds were counter screened at 5-HT$_{1A}$R because there are well-known parallels between 5-HT$_7$R and 5-HT$_{1A}$R, including their overlapping distributions in the CNS, sequence homology similarities [1], and data highlighting similarity in the putative binding sites of both receptors [34]. The assays were performed via the displacement of [^{3}H]-5-CT for 5-HT$_7$R and [^{3}H]-8-OH-DPAT for 5-HT$_{1A}$R from the cloned human receptors stably expressed in HEK293 cells.

The binding data of the analogs of compound **1a** in which various aromatic systems replaced the terminal pyrazine ring are listed in Table 1. The 5-HT$_7$R affinity values of the new compounds are distributed in a narrow range (15.7 nM < K_i < 44.3 nM) around the affinity value of **1a** (K_i = 16.1 nM) indicating that the modification of the terminal fragment was well tolerated, even when the bulky biphenyl-like phenyl-imidazo[1,2-*a*]pyridine system was introduced (**1e**).

As for 5-HT$_{1A}$R, the replacement of the pyrazine ring in **1a** reduced the affinity leading to a favorable increase of selectivity for 5-HT$_7$R, except for compound **1g**. Among the compounds featuring the 2-hydroxypropyloxy chain, **1d** and **1e** showed the highest selectivity values (26- and 49-fold, respectively).

The formal replacement of the 2-hydroxypropyloxy chain in compounds **1a–g** with the butyloxy chain provided compounds **7a–g** (Table 2). This modification was well tolerated, as the pairs of analogs displayed very close K_i values at 5-HT$_7$R, with the greatest variation in the case of the analogs **1b** and **7b** (1.7-fold).

As for 5-HT$_{1A}$R, this modification led to a decrease of affinity in all cases but **7e** and **7f**. Consequently, compounds **7b**–**d** showed increased selectivity for 5-HT$_7$R (> 20-fold) when compared to the 2-hydroxypropyloxy counterparts **1b–d**.

The third set of compounds (**14a,e** and **15a,e**) originated from **1a,e** and **7a,e**, respectively, by formally replacing the piperazine ring with a piperidine ring (Table 3). While piperidines **14a,e**, which feature the 2-hydroxypropyloxy chain, showed 5-HT_7R affinity comparable to the corresponding piperazines **1a,e**, the piperidines **15a,e**, which present the butyloxy chain, displayed 4-fold lower affinities than their piperazine counterparts **7a,e**. The replacement of the piperazine with the piperidine ring reduced the affinity for 5-HT_{1A}R, thus providing an increase in selectivity for 5-HT_7R. In particular, compound **14e** showed the best selectivity over 5-HT_{1A} receptor (76-fold) among all the studied compounds.

Finally, three different types of intermediate chains were evaluated to test their impact primarily on metabolic stability (see below) (Table 3). A six-atom chain with *gem*-dimethyl substituents in 3'- or 4'-position was well tolerated, as compounds **25** and **26** (Table 3) displayed 5-HT_7R affinity in the same range as the analog pyrazine derivatives **1a** and **7a**. Instead, the presence of the rigid triple bond linker reduced both 5-HT_7R and 5-HT_{1A}R affinities (**9** vs **7b**).

Overall, the radioligand binding data at 5-HT_7R and 5-HT_{1A}R indicated that structural elements selected for the study were compatible with 5-HT_7R affinity and, in some cases, reduced the 5-HT_{1A}R affinity. Based on 5-HT_7R and 5-HT_{1A}R affinity data, we identified compounds **1e,f**, **7c**, **7e**, **14e**, and **15e** as possible candidates for further evaluations.

In Vitro Metabolic Stability

As illustrated above, experimental in vivo data indicate that **1a** undergoes metabolic degradation. As a screening model in vitro to fulfill the aim of this study, we used rat liver microsomes, a system widely used to evaluate the susceptibility to first-pass oxidative metabolism, the main cause of metabolic degradation in vivo [35]. In the initial screening phase, the turnover of the parent compound was assessed as the percentage of the parent compound recovered after 30 min of incubation with microsomes in the presence of an NADPH-regenerating system[28,36]. Under these

experimental conditions, the recovery of unchanged **1a** was 21% (Table 1), which represented our reference value to compare and select the new compounds for further studies.

The replacement of the pyrazine group of **1a** with the selected terminal fragments had a positive effect on metabolic stability (compounds **1b–g**, Table 1). In fact, all the new compounds displayed a percentage of recovery greater than 21%, except the 2-cyanophenyl derivative **1d** which suffered from massive degradation. Also, the butyloxy derivatives **7a–g** showed percentage of recovery similar to those of the 2-hydroxypropyloxy counterparts and collectively greater than **1a** (Table 2). The replacement of the piperazine ring with the piperidine had different effects on metabolic stability. In fact, while **14a,e** and **15e** displayed percentages of recovery of parent compound similar to those of the piperazine analogs, compound **15a** was massively degraded. Finally, the metabolic stability data of compounds **25** and **26** indicated that the replacement of the 2-hydroxypropyloxy in **1a** or the butyloxy chain in **7a** introduces a soft spot in the molecule as **25** and **26** are extensively degraded under the test conditions. Instead, the presence of a triple bond in the intermediate chain does not influence the metabolic stability but reduces the affinity for 5-HT_7R (**9** vs **7b**).

Table 1. Binding affinities and microsomal stability of target compounds

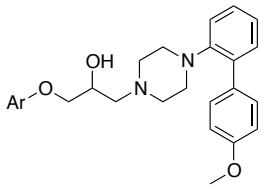

		K_i [nM] ± SEM		Microsomal stability
Compd	**Ar**	**5-HT$_7$**	**5-HT$_{1A}$**	**% rec. (30 min)**
1a	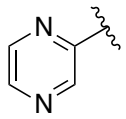	16.1 ± 0.35	82.9 ± 6.1	21
1b	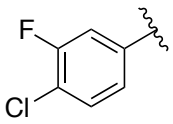	35.8 ± 7.3	449 ± 86	29
1c	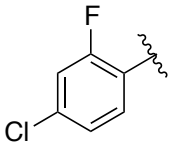	44.3 ± 7.6	264 ± 8.0	35
1d	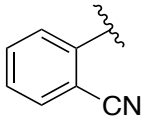	15.7 ± 0.35	403 ± 102	2
1e	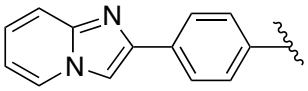	25.7 ± 2.6	1270 ± 148	48
1f	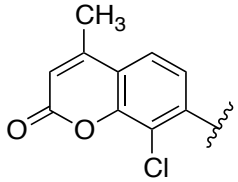	26.5 ± 7.7	475 ± 79	33
1g	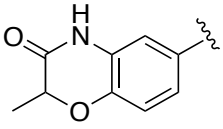	19.9 ± 1.5	8.70 ± 0.01	68

Table 2. Binding affinities and microsomal stability of target compounds

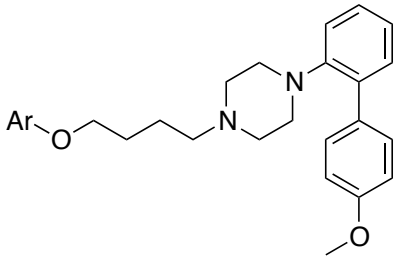

		K_i [nM] ± SEM		Microsomal stability
Compd	**Ar**	**5-HT$_7$**	**5-HT$_{1A}$**	**% rec. (30 min)**
7a	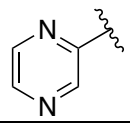	13.2 ± 2.1	197 ± 49	21
7b	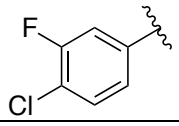	61.4 ± 8.7	2394 ± 391	35
7c	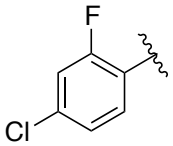	47.3 ± 7.6	967 ± 143	30
7d	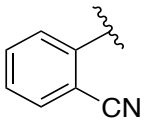	17.7 ± 5.0	477 ± 17	7
7e	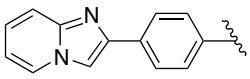	23.6 ± 5.1	521 ± 51	32
7f	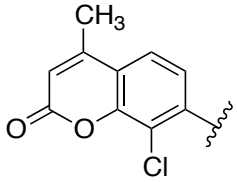	42.9 ± 6.5	135 ± 20	20
7g	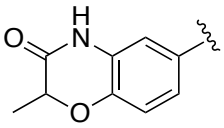	14.7 ± 0.9	127 ± 8	49

Table 3. Binding affinities and microsomal stability of target compounds

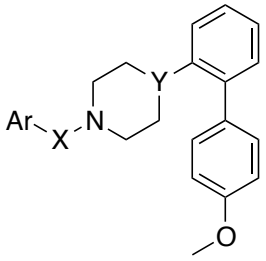

				K_i [nM] ± SEM		Microsomal stability
Compd	**Ar**	**X**	**Y**	**5-HT$_7$**	**5-HT$_{1A}$**	**% rec. (30 min)**
14a	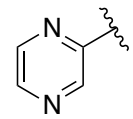	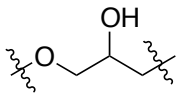	CH	15.2 ± 1.4	287 ± 39	22
14e	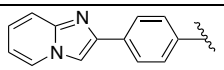	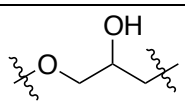	CH	36.0 ± 1.8	2750 ± 112	44
15a	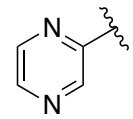	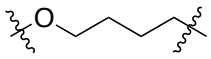	CH	45.8 ± 4.9	811 ± 42	6
15e	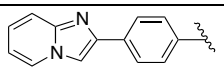	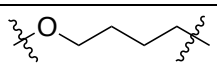	CH	74.5 ± 1.8	1370 ± 139	58
25	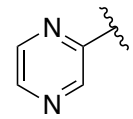		N	25.1 ± 5.6	264 ± 9.5	< 2
26	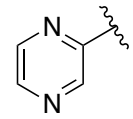	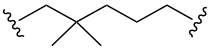	N	62.8 ± 12.8	105 ± 6.0	< 2
9	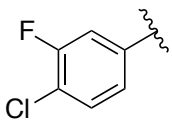		N	410 ± 50	>8000	22

Collectively, the metabolic stability data provide support to the design strategy that may lead to compounds with improved metabolic stability. In fact, 15 out of 20 of the new compounds display metabolic stability greater than **1a**.

As the next step, the most stable compounds **1c,e–g**, **7c,e,g**, **14e**, and **15e** (recovery > 30%) were further characterized in rat liver microsomes by evaluating half-life ($t_{1/2}$) and apparent intrinsic clearance ($CL_{int,\ app}$) which predict hepatic clearance in vivo [37]. All selected compounds showed improved microsomal stability with longer half-lives and $CL_{int,\ app}$ values lower than **1a** (Table 4). Interestingly, all compounds showed $CL_{int,\ scaled}$ values below 45 mL/min/Kg, which is considered the threshold for high clearance compounds [38].

With the affinity and metabolic stability data in hands, we selected a smaller set of compounds to further characterization. Among compounds **1c,e–g**, **7c,e,g**, **14e**, and **15e**, we triaged **1c**, **7b,c**, **15e** because they showed the lowest 5-HT_7R affinity values within the subset. Then, we excluded **1g** because it was a 5-HT_{1A}R-preferring ligand. The focused set of compounds then included:

i) **1e** and **14e** because they showed the best combination of 5-HT_7R affinity, selectivity, and metabolic stability;

ii) **7g** because it showed the highest 5-HT_7R affinity of the subset and was the best, within the subset, in term of metabolic stability.

Then, we assessed the metabolic stability also in cryopreserved rat hepatocytes of compounds **1e, 7g**, **14e**, and **1a** for comparative purpose. The evaluation using hepatocytes provides a better prediction of the in vivo hepatic clearance as compared to microsomes because it gives additional mechanistic insights on the metabolic processes to which a compound is subjected. $CL_{int,\ app}$ values from microsome and hepatocytes are very similar when a compound undergoes mainly CYP-mediated pathways. Instead, when a compound is subjected to non-CYP mediated metabolic pathways, higher rates of metabolism are observed in hepatocytes compared to microsomes, due to

the presence of enzymes and cofactors that are absent in microsomes. In addition, a compound displays lower apparent intrinsic clearance in hepatocytes as compared to microsomes when its interaction with uptake or efflux transporters present on hepatocyte membrane is a rate-limiting step for the intracellular entry [39].

Half-lives and apparent intrinsic clearance in hepatocytes of compounds **1e, 7g**, and **14e** (Table 4) are in agreement with the data observed in microsomes as all the studied compounds are more stable than **1a** (Table 4). It can be also noted that hepatocytes apparent intrinsic clearance of compounds **1e** and **14e** was slightly higher than that observed in microsomes, suggesting that non-CYP-mediated pathways contributed to metabolic degradation of the compounds. Also, it is reasonable to exclude rate-limiting interactions of compounds **1e** and **14e** with efflux systems on hepatocytes membranes as none of the compounds showed microsomal intrinsic clearance higher than that observed in hepatocytes.

Plasma Protein binding

Plasma protein binding was assessed as an estimation of plasma unbound fraction (f_u). Compounds **1a,e–g**, **7g**, and **14e** were tested for interaction with plasma proteins at a concentration of 10 μM, and the binding data are shown in Table 4. All the tested compounds showed a very high percentage of plasma protein binding (> 98.5%), which is predictive of very low f_u in vivo. On the other hand, high plasma protein binding limits the partitioning of the compound between the blood and the tissue where the metabolic degradation occurs and thus extends the half-life of the compound. Of note, the arylpiperazine-based antipsychotic drugs lurasidone and aripiprazole display very high plasma protein binding (>99.5%) [40,41], in the same range as our tested compounds.

Table 4. Half-life and Intrinsic Clearance of Selected Compounds

	rat microsomes			rat hepatocytes		
Compd	**$t_{1/2}$ (min)**	**$CL_{int, app}$ (μL/min/mg)**	**$CL_{int, scaled}$ (mL/min/Kg)**	**$t_{1/2}$ (min)**	**$CL_{int, scaled}$ (mL/min/Kg)**	**% plasma protein binding**
1a	30	23.1	56.1	133	76.4	98.5
1c	58	12	29	NT	NT	NT
1e	60	11.5	28.1	165	61.6	99.9
1f	38	18	44.3	147	69.1	99.4
1g	74	9.4	22.8	NT	NT	99.9
7c	63	11	26.7	NT	NT	NT
7e	58	12	29	NT	NT	NT
7g	63	11	26.7	288	35.3	98.8
14e	56	12.4	30.1	182	55.9	98.5
15e	90	7.7	18.7	NT	NT	NT

In vitro Toxicity

At this stage of the study, compounds **1e**, **7g**, and **14e** were tested for in vitro cytotoxicity, which is becoming an integral aspect of drug discovery as it is a convenient, cost-effective, and predictive tool for assessing the toxic potential of new chemical entities. The effect of compounds **1e**, **7g**, and **14e** on cell viability was assessed by using the 3-(4,5-dimethylthiazol-2-yl)-2,5-diphenyl tetrazolium bromide (MTT) assay (Table 5). As tissue-specific differences in basal toxicity exist [42], the test was performed using cell lines from different tissues. We selected neuroblastoma SY-SH5Y cell line as a model to assess neuronal toxicity, human hepatoblastoma HepG2 cell line as a model of hepatotoxicity, and the breast cancer MCF7 cell line, which is routinely used for assessing chemicals cytotoxicity. In HepG2 and MCF7 cell lines, the rank order of cytotoxicity was **14e** > **7g** > **1e**, being the latter devoid of cytotoxic effect (EC_{50} > 100 μM). whereas **7g** and **14e** showed cytotoxic effects at high concentrations, with EC_{50} values about 2–3 orders of magnitude higher than their K_i values toward 5-HT_7R. In SY-SH5Y cells, the rank order of cytotoxicity was **14e** > **1e** ≃ **7g**, with EC_{50} values slightly lower than that observed in HepG2 and MCF7 cell lines. This

behavior can be explained considering that neuronal cells are sensitive to chemicals and slight disturbances in energy metabolism may be critical for survival. Of note, amitriptyline, a marketed CNS drug, showed cytotoxic effects in SH-SY5Y and HepG2 cells similar to our compounds (SH-SY5Y IC_{50} = 48.1 μM, HepG2 IC_{50} = 29.6 μM assessed as ATP measurement after 24h drug exposure) [43].

Table 5. *In vitro* cytotoxicity, measured by MTT reduction, in different cell lines exposed for 48 h at different concentration of selected compounds.

	EC_{50} [μM]		
Compound	**MCF7**	**HepG2**	**SH-SY5Y**
1e	>100	>100	13.4
7g	24.7 ± 1.3	21.7 ± 2.3	14.8
14e	5.82 ± 1.7	2.72 ± 0.2	3.62

Next, we evaluated in vitro cardiotoxicity by assessing the effect of compounds **1e**, **7g**, and **14e** on human ether-a-go-go-related gene (hERG) potassium channel, a critical target in cardiac safety studies of new drugs. Drug-induced inhibition of hERG can lead to a rare and potentially fatal cardiac tachyarrhythmia. For this reason, the screening of drugs on hERG is mandatory during the drug development process. Compounds **1e**, **7g**, and **14e** were tested on hERG channels using an automated patch-clamp instrument. As shown in Table 6, all the compounds are able to inhibit the hERG channel, showing IC_{50} values lower than 10 μM which is often considered the threshold value between safe and potentially cardiotoxic compounds [44]. However, the sole reliance on hERG testing can result in the most promising compounds being unnecessarily eliminated from further development [45]. For instance, the concomitant inhibition of a depolarizing ion current may mitigate hERG inhibition, thus reducing the risk of cardiac arrhythmia. Thus, we tested **1e**, **7g**, and

14e on human cardiac sodium channels expressed in HEK293T cells using conventional patch-clamp. All three compounds produced a frequency-dependent inhibition of sodium currents (Figure 3).

Collectively, electrophysiological experiments showed that compounds **1e**, **7g**, and **14e** can block heterologously expressed hERG channels in a dose-dependent manner, which may raise some concern about cardiac safety. On the other hand, the compounds are also potent sodium channel blockers, which would likely reduce the risk of torsade de pointes caused by hERG block, as this occurs for commonly used class I antiarrhythmic drugs, such as mexiletine [45,46].

Altogether, in vitro toxicity data indicate that **1e** exhibits the most favorable profile. Also compounds **7g** and **14e** do not show general toxicity issues, being compound **7g** preferable because it displays EC_{50} values in the MTT test higher than **14e** (see Table 5), combined with a lower 5-HT_7R K_i value (**7g**: 14.7 nM vs **14e**: 36.0 nM). Consequently, compounds **1a** and **7g** were further evaluated to assess their ability to mimic 5-HT_7R-mediated reversal of mGluR-LTD in mouse hippocampal slices.

Table 6. Patch Clamp Profiling of Selected Compounds Activity on hERG Cell Based Assay.

Compound	IC_{50} [μM] ± SEM	n
1e	1.907 ± 0.498	4
7g	0.448 ± 0.068	5
14e	1.863 ± 0.179	5
dofetilide	0.046 ± 0.001	2

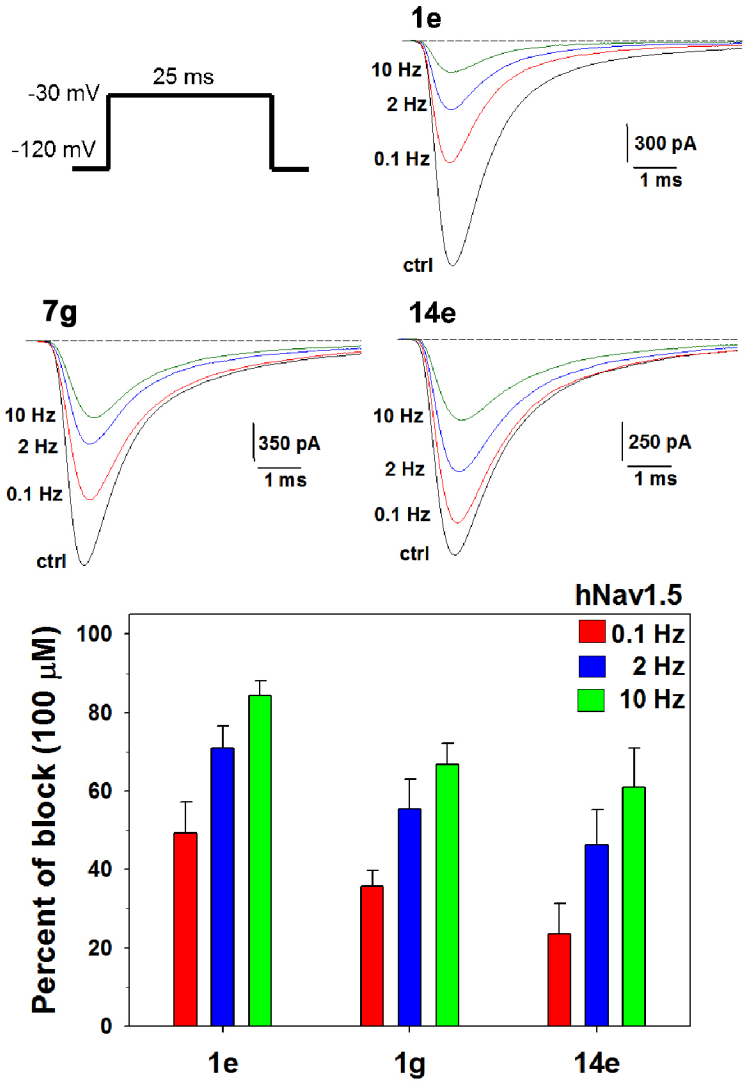

Figure 3. Effects of compounds **1e**, **7g**, and **14e** on hNav1.5 channels. Sodium currents were elicited in transfected HEK293T cells by applying a 25 ms-long test pulse at -30 mV from the holding potential of -120 mV at 0.1, 2, or 10 Hz frequency. Representative sodium current traces are shown in control condition (CTRL) and at steady-state effect of 100 μM of drug at each frequency. The bars report the mean percentage of block ± S.E.M. from 4-to-6 cells.

In vitro 5-HT$_7$R agonist activity of selected compounds

We tested the effects of **1e** on CA1 hippocampal neurons from mouse hippocampal slices, in which activation of 5-HT$_7$R is known to modulate synaptic transmission and plasticity [47]. Excitatory postsynaptic currents (EPSC) mediated by AMPA receptors were recorded under whole-cell patch clamp from CA1 pyramidal neurons following stimulation of Schaffer collaterals. mGluR-LTD was induced by bath application (5 min) of 100 μM (*S*)-3,5-dihydroxyphenylglycine (DHPG), a potent agonist of group I metabotropic glutamate receptors (Figure 4). Application of **1e** (100 nM, 5 min) after DHPG application did not significantly modify the amount of mGluR-LTD. EPSC% value (mean ± SEM) 40 min after DHPG application in control conditions was 67.7 ± 8, n= 7 neurons (from 4 animals, 2 males and 2 females) and in the presence of **1e** was 90.7 ± 13, n= 6 neurons (4 animals, 2 males and 2 females), a value that was not significantly different (P= 0.16, t= 1.469, df= 11, unpaired t-test, Figure 4A). Unfortunately, this result suggests that **1e** is not a 5-HT$_7$R agonist. Instead, application of **7g** (100 nM, 5 min) after DHPG (5 min, 100 μM) abolished mGluR-LTD: EPSC% 40 min after DHPG application in the presence of **7g** was 107 ± 8, mean ± SEM, n= 5 neurons (3 animals, 2 males and 1 female), a value significantly different from control conditions (EPSC% 67.7 ± 8, n=7 neurons; P= 0.010, t= 3.154, df= 10, unpaired t-test, Figure 4B). This result shows that **7g** is able to reverse mGluR-LTD in the mouse hippocampus. Considering that we have previously proved that reversal of mGluR-LTD by 5-HT in CA1 hippocampal neurons is mediated by activation of 5-HT$_7$R [12], we can conclude that **7g** behaves as a 5-HT$_7$R agonist in our experimental conditions. Altogether, electrophysiology studies indicated that only **7g** was suitable to be tested in *Fmr1* KO mice.

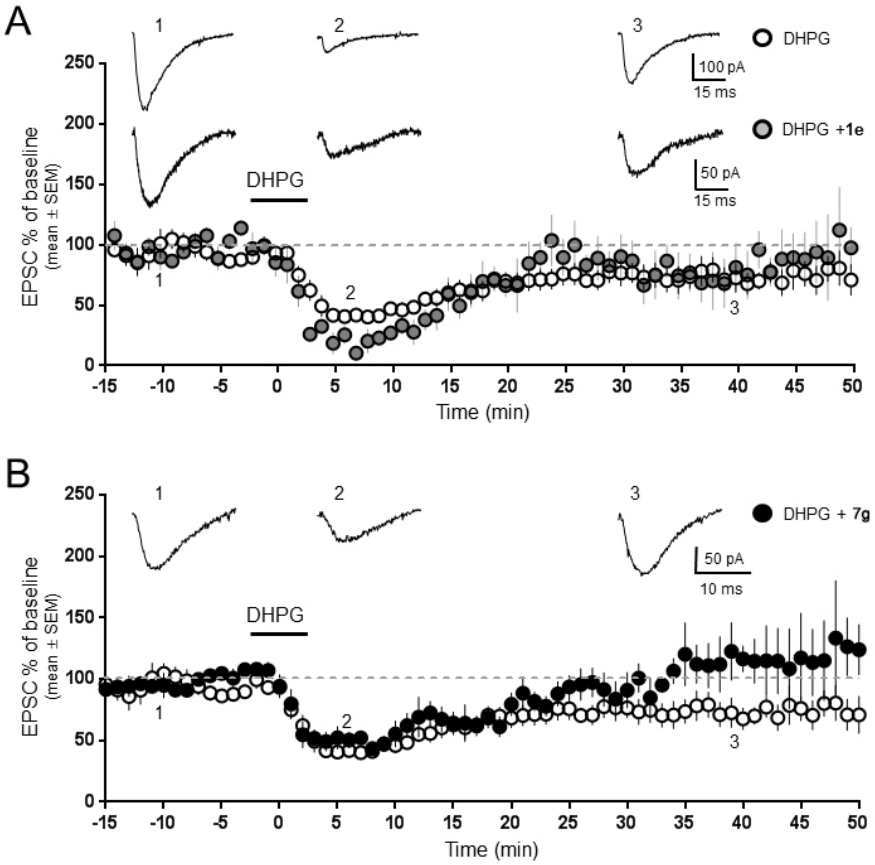

Figure 4. Effects of 5-HT_7R ligands **1e** and **7g** on mGluR-LTD induced by DHPG. Pooled data (mean ± SEM) of excitatory post synaptic current (EPSC) values (expressed as % of baseline EPSC amplitude prior to DHPG application) were plotted vs time; insets show individual EPSC traces from representative experiments. A) In control conditions (open circles), application of DHPG (100 μM, 5 min) induced mGluR-LTD: EPSC amplitude (measured 40 min after DHPG application) was 67.7 ± 8 % of baseline (n= 7 neurons from 4 animals, 2 males and 2 females). After application of **1e** (100 nM, 5 min application starting 5 min after DHPG washout), the amount of mGluR-LTD was not modified (gray circles; EPSC% 90.7 ± 13, n= 6 neurons from 4 animals, 2 males and 2 females, not significantly different from control, P= 0.16, t= 1.469, df= 11, unpaired t-test). B) After application of **7g** (100 nM, 5 min, black circles), EPSC % amplitude (107 ± 8, mean ± SEM, n= 5 neurons from 3 animals, 2 males and 1 female) was significantly different from control (P= 0.010, t= 3.154, df= 10, unpaired t-test), showing that **7g** completely reversed mGluR-LTD.

Nesting removal test in *Fmr1* KO mice

A prominent feature in autistic individuals is a strong desire to maintain sameness in a routine or their environment [48,49]. A change in routines or their environment can be quite distressing and elicit repetitive behaviors [48]. To model this in mice, we tested mice in a standard holding cage with bedding and nesting material. Time spent digging in the bedding was measured first with nesting material in the holding cage (10 min test) and subsequently with the nesting material removed from the holding cage (10 min test). Twenty-minutes prior to the test, wildtype (WT) and *Fmr1* KO (KO) mice received an ip injection of either vehicle (5% DMSO in saline) or compound **7g** at 3 mg/kg. After 20 min elapsed, a mouse was tested for digging behavior with nesting in, followed by nesting out.

An equal number of male (n= 4) and female (n= 4) mice were tested in each group. Because there was not a sex difference, male and female mice were combined into a single group for each genotype. The results from the nesting removal test are shown in Figure 5. A three-way analysis of variance (ANOVA) with repeated measures was conducted to determine an effect of genotype and/or treatment (between factors), as well as nesting condition (within factor). The analyses revealed there was a significant main effect for genotype, $F_{1,28} = 24.78$, $P < 0.0001$, reflecting KO mice spent more time digging than WT mice. There was also a significant main effect for treatment, $F_{1,28} = 9.55$, $P= 0.0045$, illustrating the effect of **7g** in reducing digging behavior. The condition factor (nesting in, nesting out) was significant, $F_{1,28} = 50.44$, $P < 0.0001$, reflecting that all groups showed an increase in digging behavior in the nesting out test compared to that in the nesting in test. Moreover, there was a significant three-way interaction, $F_{1,28} = 4.46$, $P = 0.0438$. Post-hoc analyses revealed that vehicle-treated KO mice had a significantly greater amount of digging behavior during nesting out test vs. nesting in test ($P < 0.01$). In addition, digging behavior in the nesting out test for vehicle-treated KO mice was significantly greater compared to that of all other groups (P's < 0.01). Furthermore, **7g** treatment in KO mice significantly reduced digging behavior in the nesting out test compared to that of KO mice receiving vehicle treatment ($P < 0.01$) and to a

level that was comparable to all WT groups (P's > 0.05). Thus, **7g** treatment in KO mice attenuated the elevation in a stereotyped motor behavior with a change in the environment.

The effects of **7g** treatment on locomotor activity in each genotype were examined during the nesting out test (see Figure 6). A two-way ANOVA revealed there was not a main effect for genotype, $F_{1,28}$= 2.49, P = 0.13. While there was a trend for **7g** to reduce locomotor activity in both WT and KO mice, there was not a significant effect for treatment, $F_{1,28}$ = 3.10, P = 0.09. Further, there was not a significant genotype x treatment interaction, $F_{1,28}$ = 0.53, P = 0.47.

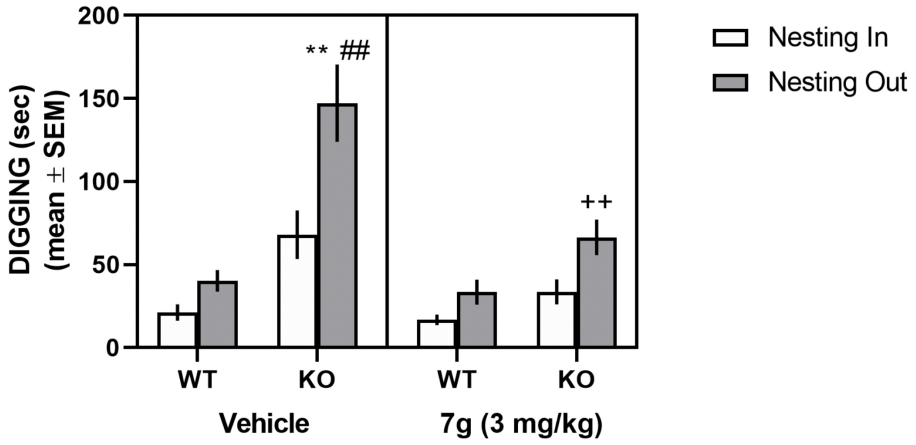

Figure 5. **7g** treatment in KO mice attenuates elevated digging behavior following removal of nesting material. The treatments on the x-axis represent the treatment received prior to the behavioral test. Vehicle-treated KO mice exhibited elevated digging behavior after removal of nesting material that was significantly greater than all other groups during the nesting out test. An ip injection of **7g** significantly reduced the elevated digging behavior in KO mice during the nesting out condition. **P <0.01 vs. KO-vehicle nesting in condition; ##P <0.01 vs. all other groups during nesting out condition. ++P < 0.01 vs. KO-vehicle group during nesting out condition.

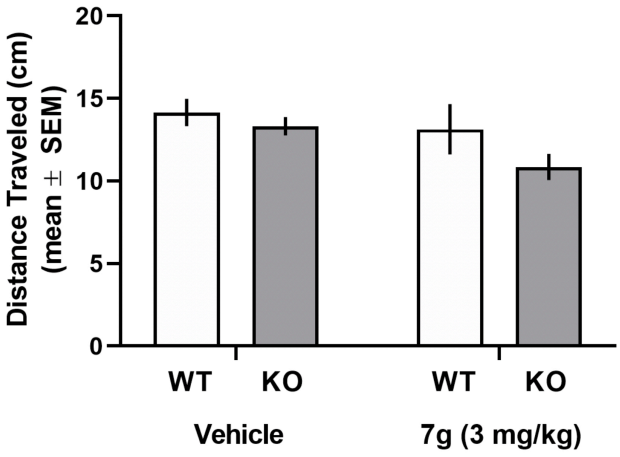

Figure 6. **7g** treatment in WT and KO mice did not affect locomotor activity during the nesting out condition. The treatments on the x-axis represent the treatment received prior to the behavioral test. There was a non-significant trend for **7g** treatment to reduce locomotor activity during the nesting out condition in both WT and KO mice (P = 0.09).

CONCLUSIONS

Recent preclinical studies have shown that activation of serotonin 5-HT_7R has the potential to treat neurodevelopmental disorders such as Fragile X syndrome which is also a rare disease. To date, a limited but increasing number of drugs for rare diseases (the so-called orphan drugs) are reaching patients. However, the majority of rare diseases are still without any effective treatment. Many initiatives worldwide exist to facilitate the transition of discoveries into therapies for rare diseases. In order to translate preclinical research results into approved orphan drugs for the benefit of patients, a rich pipeline of preclinical candidates would benefit the process. We have worked toward this goal by working on long-chain arylpiperazines, a versatile class of compounds to which several safe marketed drugs belong. In particular, following a design strategy recently proposed by Taylor and coworkers [23], we designed the new compounds exploiting privileged scaffolds (i.e., structural fragments present in clinically approved drugs or in preclinical candidates). This approach was successful because we identified a set of metabolically stable 5-HT_7R-preferring ligands. Evaluation of a subset of compounds evidenced low in vitro toxicity, providing further support to the validity of the design strategy. In fact, compounds **1e**, **7g**, and **14e** displayed an in vitro toxicity profile (MTT cytotoxicity assay, hERG blockade) comparable to that of aripiprazole

50], a representative marketed arylpiperazine drug. Among the studied compounds, we identified the drug-like 5-HT_7R agonist **7g** which is capable to rescue long-term synaptic plasticity and to attenuate stereotyped behavior in a mouse model of Fragile X syndrome. Of note, this result extends previous studies showing that activation of 5-HT_7R attenuates stereotyped behavior in a mouse model of FXS in a behavioral paradigm other than those already studied using LP-211. Additional translational preclinical studies with **7g** are in due course toward therapy for FXS.

EXPERIMENTAL SECTION

Chemistry. Chemicals were purchased from Sigma-Aldrich, Alfa Aesar, TCI Chemicals. Unless otherwise stated, all chemicals were used without further purification. Thin layer chromatography (TLC) was performed using plates from Merck (silica gel 60 F254). Column chromatography was performed with 1:30 Merck silica gel 60 Å (63-200 μm) as the stationary phase. ^{1}H NMR spectra were recorded on a Varian Mercury-VX spectrometer (300 MHz) or on a 500-vnmrs500 Agilent spectrometer (500 MHz). All chemical shift values are reported in ppm (δ). Recording of mass spectra was done on an HP6890-5973 MSD gas chromatograph/mass spectrometer; only significant *m/z* peaks, with their percentage of relative intensity in parentheses, are reported. ESI-MS/MS analysis were performed with an Agilent 1100 Series LC-MSD trap System VL workstation, mass range 50-800 *m/z*, electrospray ion source in positive or negative ion mode. All spectra were in accordance with the assigned structures. The purity of the target compounds listed in Tables 1-3 was assessed by combustion analysis and by RP-HPLC. Elemental analyses (C,H,N) of the target compounds were performed on a Eurovector Euro EA 3000 analyzer. Analyses indicated by the symbols of the elements were within ± 0.4 % of the theoretical values. RP-HPLC analysis was performed on an Agilent 1260 Infinity Binary LC System equipped with a diode array detector using a Phenomenex Gemini C-18 column (250 x 4.6 mm, 5 μm particle size). All target compounds (Tables 1-3) were eluted with CH_3CN/ammonium formate 50 mM pH 5 (4:1, v/v) at a volumetric flow rate = 1 mL/min. All compounds, except compound **25**, showed ≥ 95% purity. The following compounds were prepared as described in the literature: 8-chloro-7-hydroxy-4-methyl-chromen-2-one (**4f**) [32]; 6-hydroxy-2-methyl-2*H*-benzo[*b*][1,4]oxazin-3(4*H*)-one (**4g**) [51]; (*R*)-3-(2-cyanophenoxy)-1,2-epoxypropane (**5d**) [52]; 2-[4-(4-chlorobutoxy)phenyl]imidazo[1,2-*a*]pyridine (**6e**) [31]; 2-(4-methoxyphenyl)benzaldehyde (**10**) [53]; 3,3-dimethylpent-1,5-diol (**17**) [54]; 2,2-dimethylpentane-1,5-diol (**18**) [55]; 4-(2-pyrazinyloxy)-1-butyl methanesulfonate (**22**) [56].

General Procedure for the Preparation of Oxirane 5b-g.

To a suspension of NaH (1.1 mmol) in anhydrous DMF, cooled at 0 °C, a solution of the appropriate phenol **4b-g** (1.5 mmol) in the same solvent was added dropwise. The mixture is stirred at room temperature for 1 h, then a solution of (*R*)-glycidyl nosylate (0.41 g, 1.5 mmol) in anhydrous DMF was added. The reaction mixture was stirred at room temperature overnight, quenched with H_2O, and extracted with AcOEt (3 × 20 mL). The organic layers were collected, dried over Na_2SO_4, and concentrated under reduced pressure. The crude was purified on a silica gel column as detailed below to give pure target compound.

(*R*)-2-[(4-Chloro-3-fluorophenoxy)methyl]oxirane (5b). Eluted with *n*-hexane/EtOAc (7:3, v/v). Transparent oil, 86% yield. ^{1}H NMR ($CDCl_3$): δ 2.75 (dd, 1H, *J*= 2.8 and 4.9 Hz), 2.91 (app t, 1H), 3.31-3.38 (m, 1H), 3.84 (dd, 1H, *J*= 5.8 and 11.0 Hz), 4.23 (dd, 1H, *J*= 2.8 and 11.0 Hz), 6.63-6.74 (m, 2H), 7.22-7.28 (m, 1H). ESI$^-$/MS *m/z* 201 (M^-). ESI$^-$/MS/MS *m/z* 96 (100), 78 (61).

(*R*)-2-[(4-Chloro-2-fluorophenoxy)methyl]oxirane (5c). Eluted with *n*-hexane/EtOAc (9:1, v/v). Transparent oil, 85% yield. ^{1}H NMR ($CDCl_3$): δ 2.76 (dd, 1H, *J*= 2.8 and 5.0 Hz), 2.91 (app t, 1H), 3.34-3.39 (m, 1H), 3.98 (dd, 1H, *J*= 5.8 and 11.3 Hz), 4.28 (dd, 1H, *J*= 3.0 and 11.3 Hz), 6.88-6.98 (m, 1H), 7.01-7.12 (m, 2H). ESI$^-$/MS *m/z* 201 (M^-). ESI$^+$/MS/MS *m/z* 96 (100), 78 (61).

(*R*)-2-[4-(2-Oxiranylmethoxy)phenyl]imidazo[1,2-*a*]pyridine (5e). Eluted with $CHCl_3$/EtOAc (9:1, v/v). Pale yellow solid, 85% yield. ^{1}H NMR ($CDCl_3$): δ 2.78 (dd, 1H, *J*= 2.7 and 5.0 Hz), 2.92 (app t, 1H), 3.36-3.41 (m, 1H), 4.01 (dd, 1H, *J*= 5.8 and 11.0 Hz), 4.22 (dd, 1H, *J*= 3.3 and 11.0 Hz), 6.76 (td, 1H, *J*= 1.4 and 6.9 Hz), 6.99 (d, 2H, *J*= 8.8 Hz), 7.12-7.18 (m, 1H), 7.61 (d, 1H, *J*= 9.1 Hz), 7.78 (s, 1H), 7.90 (d, 2H, *J*= 8.8 Hz), 8.10 (dt, 1H, *J*= 1.1 and 6.6 Hz). GC/MS *m/z* 267 (M^++1, 20), 266 (M^+, 100), 209 (65), 181 (50), 78 (22).

(*R*)-8-Chloro-4-methyl-7-(2-oxiranylmethoxy)-(2*H*)-chromen-2-one (5f). Eluted with $CHCl_3$/EtOAc (7:3, v/v). White solid, 80% yield. ^{1}H NMR ($CDCl_3$): δ 2.41 (s, 3H), 2.46-2.88 (m, 1H), 2.95 (app t, 1H), 3.40-3.45 (m, 1H), 4.13 (dd, 1H, *J*= 5.5 and 11.3 Hz), 4.43 (dd, 1H, *J*= 2.8 and 11.3 Hz), 6.16 (br s, 1H), 6.94 (d, 1H, *J*= 8.8 Hz), 7.48 (d, 1H, *J*= 8.8 Hz). GC/MS *m/z* 267 (M^++1, 20), 266 (M^+, 100), 209 (65), 181 (50), 78 (22).

(2*R*)-2-Methyl-6-[(*R*)-oxiran-2-ylmethoxy]-2*H*-benzo[b][1,4]oxazin-3(4*H*)-one (5g). Eluted with *n*-hexane/EtOAc (1:1, v/v). Colourless oil, 41% yield. ^{1}H NMR ($CDCl_3$): δ 1.56 (d, 3H, *J*= 6.4 Hz), 2.73-2.76 (m, 1H), 2.90 (app t, 1H), 3.31-3.35 (m, 1H), 3.88 (dd, 1H, *J*= 5.3 and 11.1 Hz), 4.19 (dd, 1H, *J*= 2.9 and 11.1 Hz), 4.58 (q, 1H, *J*= 6.4 Hz), 6.43 (d, 1H, *J*= 2.8 Hz), 6.52 (dd, 1H, *J*= 2.9 and 8.8 Hz), 6.88 (d, 1H, *J*= 8.8 Hz), 8.44 (br s, 1H, D_2O exchanged). GC/MS *m/z* 236 (M^++1, 15), 235 (M^+, 100), 179 (40), 55 (39).

General procedure for the Preparation of Compounds 6b-g.

A mixture of the appropriate phenol **4b-g** (1.2 mmol), the alkylating agent (0.52 g, 2.4 mmol) and K_2CO_3 (0.25 g, 1.8 mmol) in acetone (20 mL) was refluxed for 5-8 h. After cooling, the solvent was evaporated under reduced pressure and the residue was partitioned between AcOEt (20 mL) and H_2O (20 mL). The organic layer was separated, dried over Na_2SO_4, and concentrated under reduced pressure. The crude was purified on a silica gel column as detailed below to give pure target compound.

4-(4-Bromobutoxy)-1-chloro-2-fluorobenzene (6b). Eluted with *n*-hexane/EtOAc (4:1, v/v). Colourless oil, quantitative yield. ^{1}H NMR ($CDCl_3$): δ 1.93-2.07 (m, 4H), 3.47 (t, 2H, *J*= 6.6 Hz), 3.95 (t, 2H, *J*= 6.6 Hz), 6.59-6.71 (m, 2H), 7.22-7.28 (m, 1H). GC/MS *m/z* 282 (M^++2, 10), 280 (M^+, 7), 146 (100), 135 (80), 55 (79).

4-(4-Bromobutoxy)-1-chloro-3-fluorobenzene (6c). Eluted with *n*-hexane/EtOAc (4/1, v/v). Colourless oil, quantitative yield. ^{1}H NMR ($CDCl_3$): δ 1.92-2.02 (m, 4H), 3.47 (t, 2H, *J*= 6.6 Hz), 3.95 (t, 2H, *J*= 6.6 Hz), 6.88-6.98 (m, 1H), 7.01-7.12 (m, 2H). GC/MS *m/z* 282 (M^++2, 10), 280 (M^+, 7), 146 (100), 135 (70), 55 (79).

2-(4-Bromobutoxy)benzonitrile (6d). Eluted with *n*-hexane/EtOAc (4:1, v/v). Colourless oil, quantitative yield. ^{1}H NMR ($CDCl_3$): δ 1.92-2.02 (m, 4H), 3.47 (t, 2H, *J*= 6.6 Hz), 3.95 (t, 2H, *J*= 6.6 Hz), 7.00-7.06 (m, 2H), 7.50-7.57 (m, 2H). GC/MS *m/z* 255 (M^++2, 5), 253 (M^+, 5), 137 (60), 135 (70), 119 (100).

7-(4-Bromobutoxy)-8-chloro-4-methyl-2*H*-chromen-2-one (6f). Eluted with *n*-hexane/EtOAc (4:1, v/v). White solid, 54% yield. ^{1}H NMR ($CDCl_3$): δ 2.01-2.15 (m, 4H), 2.41 (d, 3H, *J*= 1.1 Hz), 3.53 (t, 2H, *J*= 6.3 Hz), 4.17 (t, 2H, *J*= 6.1 Hz), 6.18 (d, 1H, *J*= 1.1 Hz), 6.99 (d, 1H, *J*= 8.8 Hz), 7.46 (d, 1H, *J*= 8.8 Hz). GC/MS *m/z* 311 (M^++2, 5), 309 (M^+, 5), 230 (60), 135 (100), 55 (30).

6-(4-Bromobutoxy)-2-methyl-2*H*-benzo[b][1,4]oxazin-3(4*H*)-one (6g). Eluted with *n*-hexane/EtOAc (1:1, v/v). White solid, 42% yield. ^{1}H NMR ($CDCl_3$): δ 1.58 (d, 3H, *J*= 6.8 Hz), 1.91-1.96 (m, 2H), 2.04-2.10 (m, 2H), 3.49 (t, 2H, *J*= 6.4 Hz), 3.95 (t, 2H, *J*= 6.4 Hz), 4.60 (q, 1H, *J*= 6.4 Hz), 6.38 (d, 1H, *J*= 2.9 Hz), 6.50 (dd, 1H, *J*= 2.6 and 8.8 Hz), 6.89 (d, 1H, *J*= 8.8 Hz), 8.24 (br s, 1H, D_2O exchanged). GC/MS *m/z* 315 (M^++2, 21), 313 (M^+, 22), 179 (80), 137 (98), 135 (100), 55 (90).

4-[(4-Bromobut-2-yn-1-yl)oxy]-1-chloro-2-fluorobenzene (8). Eluted with *n*-hexane/EtOAc (1:1, v/v). Pale brown oil, 80% yield. ^{1}H NMR ($CDCl_3$): δ 3.92 (app t, 2H), 4.72 (app t, 2H), 6.59-6.71 (m, 2H), 7.22-7.28 (m, 1H). GC/MS *m/z* 278 (M^++2, 10), 276 (M^+, 7), 197 (50), 162 (100), 146 (51).

3-[2-(4-Methoxyphenyl)phenyl]pentanedioic acid (11). A solution of 2-(4-methoxyphenyl)benzaldehyde (**10**) (0.99 g, 4.69 mmol), ethyl acetoacetate (1.19 mL, 9.38 mmol) and piperidine (0.1 mL, 0.94 mmol) in EtOH (5 mL) were stirred at room temperature for 15 h. Then, 12 M NaOH (15 mL) and EtOH (15 mL) were added to the reaction mixture and the solution was refluxed for 4 h. After cooling, the organic phase was removed, and the aqueous layer was acidified with concd. HCl and extracted with AcOEt (2 × 30 mL). The organic layers were washed with water and brine, dried over Na_2SO_4, and concentrated under reduced pressure. The residue was washed with cold EtO_2 to give the pure compound as a white solid (0.42 g, 29% yield). ^{1}H NMR (CD_3OD): δ 2.58 (d, 4H, *J*= 5.2 Hz), 3.24-3.38 (m, 1H), 3.82 (s, 3H), 6.91-6.99 (m, 2H), 7.08-7.15 (m, 1H), 7.16-7.23 (m, 1H), 7.25-7.30 (m, 3H), 7.33-7.40 (m, 1H). ESI$^-$/MS *m/z* 313 (M^-). ESI$^-$/MS/MS *m/z* 269 (100).

4-[2-(4-Methoxyphenyl)phenyl]piperidine-2,6-dione (12). A mixture of the 1,5-pentanedioic acid (**11**) (0.21 g, 0.66 mmol) and urea (0.048 g, 0.79 mmol) was heated at 160–165 °C for 2 h. After cooling, the reaction mixture was dissolved in $CHCl_3$ and washed with water. The organic layer was separated dried over Na_2SO_4 and concentrated under reduced pressure. The crude was purified on a silica gel column, using $CHCl_3$/EtOAc (1:1, v/v) as eluent, to obtain the desired compound as a white solid (0.14 g, 72% yield). ^{1}H NMR ($CDCl_3$): δ 2.53-2.90 (m, 4H), 3.51-3.66 (m, 1H), 3.82 (s, 3H), 6.86-6.99 (m, 2H), 7.09-7.18 (m, 2H), 7.25-7.30 (m, 3H), 7.33-7.40 (m, 1H), 8.08 (br s, 1H, D_2O exchanged). GC/MS *m/z* 296 (M^++1, 120), 295 (M^+, 100), 208 (35), 165 (30).

4-[2-(4-Methoxyphenyl)phenyl]piperidine (13). A solution of the imide **12** (0.14 g, 0.46 mmol) in anhydrous THF was added dropwise to a cooled suspension of $LiAlH_4$ (0.05 g, 1.21 mmol) in the same solvent. The resulting suspension was stirred under reflux for 3 h. Then, the mixture was cooled at 0 °C, and a few drops of H_2O were added to destroy the excess hydride. The mixture was

filtered, and the solvent was evaporated under reduced pressure. The residue was taken up with AcOEt and washed first with H_2O and then brine. The organic layer was separated, dried over Na_2SO_4, and concentrated under reduced pressure. The crude residue was chromatographed using $CHCl_3$/MeOH (19:1, v/v) as eluent, to give pure **13** as a colorless oil in quantitative yield. ^{1}H NMR ($CDCl_3$): δ 1.62-1.66 (m, 4H), 1.85 (br s, 1H, D_2O exchanged), 2.43-2.48 (m, 2H), 2.73-2.82 (m, 1H), 3.02-3.08 (m, 2H), 3.82 (s, 3H), 6.86-6.99 (m, 2H), 7.09-7.18 (m, 2H), 7.25-7.30 (m, 3H), 7.33-7.40 (m, 1H). GC/MS *m/z* 268 (M^++1, 5), 267 (M^+, 335), 165 (34), 56 (100).

General Procedure for the Preparation of Compounds 19-21.

To a suspension of NaH (0.1 g, 4.2 mmol) in anhydrous DMF (2 mL), cooled at 0 °C, a mixture of 2-chloropyrazine (0.19 mL, 2.2 mmol) and the appropriate alkyldiol **16-18** (3.7 mmol) dissolved in the same solvent (4 mL) was added dropwise. The reaction mixture was stirred at room temperature overnight, quenched with H_2O, and extracted with AcOEt (3 × 20 mL). The combined organic layers were dried over Na_2SO_4 and concentrated under reduced pressure. The crude residue was purified on a silica gel column as detailed below to give pure target compound.

4-(2-Pyrazinyloxy)-1-butanol (19). Eluted with *n*-hexane/EtOAc (1:1, v/v). Pale yellow oil, 40% yield. ^{1}H NMR ($CDCl_3$): δ 1.67-1.73 (m, 2H), 1.83-1.90 (m, 2H), 2.42 (br s, 1H, D_2O exchanged), 3.68 (t, 2H, *J*= 6.3 Hz), 4.31 (t, 2H, *J*= 6.3 Hz), 7.96-8.06 (m, 2H), 8.16 (d, 1H, *J*= 1.4 Hz). GC/MS *m/z* 169 (M^++1, 1), 168 (M^+, 10), 96 (100), 68 (80).

3,3-Dimethyl-5-(2-pyrazinyloxy)-1-pentanol (20). Eluted with $CHCl_3$/EtOAc (9:1, v/v). Pale yellow oil, 24% yield. ^{1}H NMR ($CDCl_3$): δ 1.01 (s, 6H), 1.43 (br s, 1H, D_2O exchanged), 1.60-1.64 (m, 2H), 1.77 (t, 2H, *J*= 7.4 Hz), 3.75 (app t, 2H), 4.39 (t, 2H, *J*= 7.4 Hz), 8.06-8.10 (m, 2H), 8.18 (d, 1H, *J*= 1.1 Hz). ESI$^+$/MS *m/z* 233 (M-Na^+). ESI$^+$/MS/MS *m/z* 176 (100), 119 (80).

2,2-Dimethyl-5-(pyrazin-2-yloxy)pentan-1-ol (21). Eluted with $CHCl_3$/EtOAc (9:1, v/v). Pale yellow oil, 23% yield. ^{1}H NMR ($CDCl_3$): δ 1.01 (s, 6H), 1.43 (br s, 1H, D_2O exchanged), 1.60-1.64 (m, 2H), 1.77-1.81 (m, 2H), 3.45 (s, 2H) 4.11 (t, 2H, *J*= 7.4 Hz), 8.06-8.10 (m, 2H), 8.18 (d, 1H, *J*= 1.1 Hz). GC/MS *m/z* 211 (M^++1, 1), 210 (M^+, 10), 97 (100), 55 (80).

General Procedure for the Preparation of Methanesulfonates 22-24.

To a solution of the appropriate alcohol **19-21** (1.7 mmol) in CH_2Cl_2 (10 mL), cooled at -10 °C, Et_3N (0.35 mL, 2.54 mmol) and methanesulfonyl chloride (0.26 mL, 3.4 mmol) were added dropwise. The mixture was stirred at room temperature for 5 h. Then, the reaction mixture was first washed with a saturated aqueous solution of $NaHCO_3$, and then with 3 N HCl. The separated organic layer was dried over Na_2SO_4 and concentrated under reduced pressure. The crude residue was purified on a silica gel column as detailed below to give the pure target compound.

4-(2-Pyrazinyloxy)-1-butyl methanesulfonate (22). Eluted with *n*-hexane/EtOAc (1:1, v/v). Pale yellow oil, 40% yield. ^{1}H NMR ($CDCl_3$): δ 1.91-2.07 (m, 4H), 3.03 (s, 3H), 4.31 (app t, 2H), 4.49 (app t, 2H), 8.22 (d, 1H, *J*= 2.4 Hz), 8.32 (s, 1H), 8.48 (d, 1H, *J*= 2.4 Hz). GC/MS *m/z* 247 (M^++1, 1), 246 (M^+, 10), 151 (25), 96 (100), 79 (60).

3,3-Dimethyl-5-(2-pyrazinyloxy)-1-pentyl methanesulfonate (23). Eluted with $CHCl_3$/EtOAc (9:1, v/v). Pale yellow oil, quantitative yield. ^{1}H NMR ($CDCl_3$): δ 1.01 (s, 6H), 1.60-1.64 (m, 2H), 1.77 (t, 2H, *J*= 7.4 Hz), 3.10 (s, 3H), 4.31 (app t, 2H), 4.49 (app t, 2H), 8.22 (d, 1H, *J*= 2.4 Hz), 8.32 (s, 1H), 8.48 (d, 1H, *J*= 2.4 Hz). ESI$^+$/MS *m/z* 311 (M-Na^+). ESI$^+$/MS/MS *m/z* 215 (42), 193 (100).

2,2-Dimethyl-5-(pyrazin-2-yloxy)-1-pentyl methanesulfonate (24). Eluted with $CHCl_3$/EtOAc (9:1, v/v). Pale yellow oil, quantitative yield. ^{1}H NMR ($CDCl_3$): δ 1.01 (s, 6H), 1.60-1.64 (m, 2H),

1.75-1.78 (m, 2H), 3.10 (s, 3H), 3.85 (s, 2H) 4.21 (t, 2H, *J*= 7.4 Hz), 8.22 (d, 1H, *J*= 2.4 Hz), 8.32 (s, 1H), 8.48 (d, 1H, *J*= 2.4 Hz). ESI^+/MS *m/z* 311 ($M\text{-}Na^+$). ESI^+/MS/MS *m/z* 215 (42), 193 (100).

General Procedure for the Preparation of Final Compounds 1b–g, and 14a,e.

A mixture of the 1-[2-(4-methoxyphenyl)phenyl]piperazine or piperidine **13** (1.2 mmol) and the epoxide **5b–g** (1.0 mmol) in 20 mL of ethanol was refluxed for 5 hours. After cooling, the solvent was removed in vacuo. The crude residue was chromatographed as detailed below to give desired pure compound.

(*R*)-1-(4-Chloro-3-fluorophenoxy)-3-[4-[2-(4-methoxyphenyl)phenyl]piperazin-1-yl]propan-2-ol (1b). Eluted with $CHCl_3$/AcOEt (7:3, v/v). Pale yellow oil, 43% yield. ^1H NMR ($CDCl_3$): δ 2.38-2.40 (m, 3H, 1H D_2O exchanged), 2.48-2.52 (m, 2H), 2.56-2.62 (m, 2H), 2.82-2.92 (m, 4H), 3.85 (s, 3H), 3.92-3.93 (m, 2H), 3.99-4.08 (m, 1H), 6.64-6.75 (m, 2H), 6.94 (d, 2H, *J*= 8.8 Hz), 7.08-7.09 (m, 2H), 7.21-7.33 (m, 3H), 7.58 (d, 2H, *J*= 8.8 Hz). ESI-MS *m/z* 471 $(M+H)^+$. ESI-MS/MS *m/z* 266 (83), 226 (100). Anal. ($C_{26}H_{28}ClFN_2O_3$•HCl) C, H, N.

(*R*)-1-(4-Chloro-2-fluorophenoxy)-3-[4-[2-(4-methoxyphenyl)phenyl]piperazin-1-yl]propan-2-ol (1c). Eluted with $CHCl_3$/AcOEt (7:3, v/v). Pale yellow oil, 80% yield. ^1H NMR ($CDCl_3$): δ 2.38-2.49 (m, 3H, 1H D_2O exchanged), 2.52-2.55 (m, 2H), 2.59-2.61 (m, 2H), 2.86-2.91 (m, 4H), 3.85 (s, 3H), 4.00-4.02 (m, 2H), 4.03-4.10 (m, 1H), 6.89-6.96 (m, 3H), 7.01-7.11 (m, 4H), 7.21-7.29 (m, 2H), 7.58 (d, 2H, *J*= 8.8 Hz). ESI-MS *m/z* 471 $(M+H)^+$. ESI-MS/MS *m/z* 266 (83), 226 (100). Anal. ($C_{26}H_{28}ClFN_2O_3$•HCl) C, H, N.

(*R*)-2-[2-Hydroxy-3-[4-[2-(4-methoxyphenyl)phenyl]piperazin-1-yl]propoxy]benzonitrile (1d). Eluted with $CHCl_3$/AcOEt (1:1, v/v). Pale yellow oil, 80% yield. ^1H NMR ($CDCl_3$): δ 1.61 (br s, 1H, D_2O exchanged), 2.38-2.42 (m, 2H), 2.62-2.68 (m, 4H), 2.84-2.88 (m, 4H), 3.87 (s, 3H), 4.09-

4.16 (m, 3H), 6.96 (d, 2H, *J*= 8.8 Hz), 7.01-7.04 (m, 2H), 7.06-7.09 (m, 2H), 7.23-7.29 (m, 2H), 7.52-7.57 (m, 2H), 7.60 (d, 2H, *J*= 8.8 Hz). ESI-MS *m/z* 444 $(M+H)^+$. ESI-MS/MS *m/z* 266 (100), 219 (79). Anal. ($C_{27}H_{29}N_3O_3$•HCl•H_2O) C, H, N.

(*R*)-1-[4-(Imidazo[1,2-a]pyridin-2-yl)phenoxy]-3-[4-[2-(4-methoxyphenyl)phenyl]piperazin-1-yl]propan-2-ol (1e). Eluted with $CHCl_3$/AcOEt (7:3, v/v). White solid, 57% yield. ^{1}H NMR ($CDCl_3$): δ 1.65 (br s, 1H, D_2O exchanged), 2.39-2.41 (m, 2H), 2.51-2.61 (m, 4H), 2.83-2.92 (m, 4H), 3.85 (s, 3H), 4.01-4.13 (m, 3H), 6.76 (td, 1H, *J*= 1.1 and 6.6 Hz), 6.92-7.09 (m, 8H), 7.12-7.18 (m, 1H), 7.21-7.24 (m, 1H), 7.61 (d, 2H, *J*= 9.1 Hz), 7.78 (s, 1H), 7.86 (d, 2H, *J*= 8.8 Hz), 8.10 (d, 1H, *J*= 6.6 Hz). ESI-MS *m/z* 535 $(M+H)^+$. ESI-MS/MS *m/z* 325 (100), 224 (12). Anal. ($C_{33}H_{34}N_4O_3$•2HCl•H_2O) C, H, N.

(*R*)-8-Chloro-7-[2-hydroxy-3-[4-[2-(4-methoxyphenyl)phenyl]piperazin-1-yl]propoxy]-4-methyl-2*H*-chromen-2-one (1f). Eluted with $CHCl_3$/AcOEt (7:3, v/v). White solid, 66% yield. ^{1}H NMR ($CDCl_3$): δ 1.58 (br s, 1H, D_2O exchanged), 2.04 (s, 3H), 2.40-2.47 (m, 2H), 2.56-2.67 (m, 4H), 2.83-2.92 (m, 4H), 3.85 (s, 3H), 4.08-4.14 (m, 3H), 6.18 (d, 1H, *J*= 1.1 Hz), 6.91-6.95 (m, 3H), 7.01-7.09 (m, 2H), 7.19-7.23 (m, 2H), 7.45 (d, 1H, *J*= 8.8 Hz), 7.55-7.60 (m, 2H). ESI-MS *m/z* 557 $(M+Na)^+$. ESI-MS/MS *m/z* 347 (46), 325 (100). Anal. ($C_{30}H_{31}ClN_2O_5$•HCl) C, H, N.

6-{(*R*)-2-Hydroxy3-[4-[2-(4-methoxyphenyl)phenyl]piperazin-1-yl]propoxy}-2-methyl-2*H*-benzo[b][1,4]oxazin-3(4*H*)-one (1g). Eluted with $CHCl_3$/AcOEt (1:1, v/v). White semisolid, 30% yield. ^{1}H NMR ($CDCl_3$): δ 1.62 (br s, 1H, D_2O exchanged), 1.47 (d, 3H, *J*= 6.8 Hz), 2.30-2.32 (m, 2H,), 2.39-2.45 (m, 2H), 2.48-2.54 (m, 2H), 2.79-2.83 (m, 4H), 3.78 (s, 3H), 3.82 (d, 2H, *J*= 4.9 Hz), 3.94-3.97 (m, 1H), 4.49 (q, 1H, *J*= 6.8 Hz), 6.79 (d, 1H, *J*= 8.8 Hz), 6.84-6.87 (m, 2H), 6.94 (dd, 1H, *J*= 1.1 and 8.3 Hz), 6.99 (td, 1H, *J*= 1.5 and 7.3 Hz), 7.14-7.20 (m, 4H), 7.48-7.51 (m,

2H), 8.35 (br, 1H, D_2O exchanged). ESI-MS *m/z* 526 $(M+Na)^+$. ESI-MS/MS *m/z* 526 (100), 347 (11). Anal. ($C_{29}H_{33}N_3O_5$•HCl) C, H, N.

(*R*)-1-[4-[2-(4-Methoxyphenyl)phenyl]piperidin-1-yl]-3-(pyrazin-2-yloxy)-2-propanol (14a). Eluted with $CHCl_3$/AcOEt (1:1, v/v). Pale yellow oil, 60% yield. ^1H NMR ($CDCl_3$): δ 1.73 (br s, 1H, D_2O exchanged), 1.76-1.86 (m, 3H), 1.88-1.95 (m, 2H), 2.22-2.26 (m, 1H), 2.42 (dd, 1H, *J*= 3.9 and 12.7 Hz), 2.52 (dd, 1H, *J*= 12.3 Hz), 2.70-2.74 (m, 1H), 2.88 (d, 1H, *J*= 11.2 Hz), 3.05 (d, 1H, *J*= 11.2 Hz), 3.88 (s, 3H), 4.10-4.13 (m, 1H), 4.28 (dd, 1H, *J*= 11.2 Hz), 4.41 (dd, 1H, *J*= 3.4 and 11.2 Hz), 6.94-6.97 (m, 2H), 7.12-7.24 (m, 4H), 7.32-7.36 (m, 1H), 7.38-7.40 (m, 1H), 8.05 (dd, 1H, *J*= 1.5 and 2.9 Hz), 8.13 (d, 1H, *J*= 2.9 Hz), 8.29 (d, 1H, *J*= 1.5 Hz). ESI-MS *m/z* 442 $(M+Na)^+$. ESI-MS/MS *m/z* 324 (100). Anal. ($C_{25}H_{29}N_3O_3$•2HCl) C, H, N.

(*R*)-[4-(Imidazo[1,2-a]pyridin-2-yl)phenoxy]-3-[4-[2-(4-methoxyphenyl)phenyl]piperidin-1-yl]propan-2-ol (14e). Eluted with $CHCl_3$/AcOEt (1:1, v/v). Pale yellow solid, 38% yield. ^1H NMR ($CDCl_3$): δ 1.71 (br s, 1H, D_2O exchanged), 1.76-1.85 (m, 3H), 1.87-1.95 (m, 2H), 2.22-2.25 (m, 1H), 2.50 (dd, 1H, *J*= 3.9 and 12.2 Hz), 2.56 (dd, 1H, *J*= 12.2 Hz), 2.70-2.74 (m, 1H), 2.91 (d, 1H, *J*= 11.2 Hz), 3.07 (d, 1H, *J*= 11.2 Hz), 3.88 (s, 3H), 4.03 (d, 2H, *J*= 5.4 Hz), 4.11-4.14 (m, 1H), 6.77 (td, 1H, *J*= 1.0 and 6.9 Hz), 6.95-6.98 (m, 2H), 6.99-7.01 (m, 2H), 7.11-7.18 (m, 2H), 7.19-7.25 (m, 3H), 7.35 (td, 1H, *J*= 1.5 and 7.8 Hz), 7.40 (dd, 1H, *J*= 1.0 and 7.8 Hz), 7.61-7.63 (m, 1H), 7.79 (s, 1H), 7.87-7.89 (m, 2H), 8.11-8.12 (m, 1H). ESI-MS *m/z* 556 $(M+Na)^+$. ESI-MS/MS *m/z* 346 (100), 289 (70). Anal. ($C_{34}H_{35}N_3O_3$•HCl•H_2O) C, H, N.

General Procedure for the Preparation of Final Compounds 7a-g, 9, 15a,e, 25, and 26. A stirred mixture of the alkylating agent **6b-g**, **8**, and **22-24** (0.7 mmol), the 1-[2-(4-methoxyphenyl)phenyl]piperazine or piperidine **13** (0.6 mmol) and K_2CO_3 (0.1 g, 0.7 mmol) in acetonitrile (20 mL) was refluxed overnight. After cooling, the mixture was evaporated to dryness,

and H_2O (20 mL) was added to the residue. The aqueous phase was extracted with AcOEt (2 × 30 mL). The collected organic layers were dried over Na_2SO_4 and evaporated under reduced pressure. The crude residue was purified by chromatographic column as detailed below to afford pure target compound.

2-[4-[4-[2-(4-Methoxyphenyl)phenyl]piperazin-1-yl]butoxy]pyrazine (7a). Eluted with $CHCl_3$/AcOEt (1:1, v/v). Pale yellow oil, 39% yield. ^{1}H NMR ($CDCl_3$): δ 1.60-1.68 (m, 2H), 1.75-1.82 (m, 2H,), 2.38 (app t, 6H), 2.86 (app t, 4H), 3.85 (s, 3H), 4.31 (t, 2H, *J*= 6.3 Hz), 6.92-6.96 (m, 2H), 7.01-7.07 (m, 2H), 7.20-7.24 (m, 2H), 7.55-7.59 (m, 2H), 8.04-8.06 (m, 1H), 8.08 (d, 1H, *J*= 3.0 Hz), 8.19 (d, 1H, *J*= 1.4 Hz). ESI-MS *m/z* 441 $(M+Na)^+$. ESI-MS/MS *m/z* 323 (100). Anal. ($C_{25}H_{30}N_4O_2$•2HCl) C, H, N.

1-[4-(4-Chloro-3-fluorophenoxy)butyl]-4-[2-(4-methoxyphenyl)phenyl]piperazine (7b). Eluted with $CHCl_3$/AcOEt (1:1, v/v). Pale yellow oil, 41% yield. ^{1}H NMR ($CDCl_3$): δ 1.59-1.68 (m, 2H), 1.73-1.82 (m, 2H,), 2.37 (app t, 6H), 2.87 (app t, 4H), 3.85 (s, 3H), 3.92 (t, 2H, *J*= 6.5 Hz), 6.62 (ddd, 1H, *J*= 2.7 and 7.7 Hz; J_{H-F}= 1.0 Hz), 6.69 (dd, 1H, *J*= 2.7 Hz; J_{H-F}= 10.7 Hz), 6.91-6.96 (m, 2H), 7.01-7.07 (m, 2H), 7.19-7.24 (m, 3H), 7.56-7.61 (m, 2H). ESI-MS *m/z* 469 $(M+H)^+$. ESI-MS/MS *m/z* 469 (52), 226 (100), 200 (75). Anal. ($C_{27}H_{30}ClFN_2O_2$•HCl) C, H, N.

1-[4-(4-Chloro-2-fluorophenoxy)butyl]-4-[2-(4-methoxyphenyl)phenyl]piperazine (7c). Eluted with $CHCl_3$/AcOEt (1:1, v/v). Pale yellow oil, 30% yield. ^{1}H NMR ($CDCl_3$): δ 1.64-1.69 (m, 2H), 1.80-1.85 (m, 2H,), 2.39 (app t, 6H), 2.87 (app t, 4H), 3.87 (s, 3H), 4.02 (t, 2H, *J*= 6.4 Hz), 6.88 (t, 1H, *J*= 8.8 Hz), 6.93-6.96 (m, 2H), 7.02-7.10 (m, 3H), 7.22-7.27 (m, 3H), 7.58-7.61 (m, 2H). ESI-MS *m/z* 491 $(M+Na)^+$. ESI-MS/MS *m/z* 323 (100). Anal. ($C_{27}H_{30}ClFN_2O_2$•2HCl) C, H, N.

2-[4-[2-(4-Methoxyphenyl)phenyl]piperazin-1-yl]butoxy]benzonitrile (7d). Eluted with $CHCl_3$/AcOEt (1:1, v/v). Pale brown oil, 27% yield. ^1H NMR ($CDCl_3$): δ 1.67-1.72 (m, 4H), 1.87 (q, 2H, *J*= 6.5 Hz), 2.40 (app t, 4H), 2.85 (app t, 4H), 3.86 (s, 3H), 4.08 (t, 2H, *J*= 6.4 Hz), 6.92-6.95 (m, 2H), 6.98 (t, 1H, *J*= 7.3 Hz), 7.01-7.06 (m, 2H), 7.21-7.22 (m, 2H), 7.23-7.26 (m, 1H), 7.50 (td, 1H, *J*= 1.5 and 7.3 Hz), 7.54-7.60 (m, 3H). ESI-MS *m/z* 464 $(M+Na)^+$. ESI-MS/MS *m/z* 323 (100). Anal. ($C_{28}H_{31}N_3O_2$•HCl•H_2O) C, H, N.

4-[3-[4-[2-(4-Methoxyphenyl)phenyl]piperazin-1-yl]butoxy]phenyl)imidazo[1,2-a]pyridine (7e). Eluted with $CHCl_3$/MeOH (98:2, v/v). Pale yellow oil, 30% yield. ^1H NMR ($CDCl_3$): δ 1.64-1.71 (m, 2H), 1.77-1.83 (m, 2H,), 2.40 (app t, 6H), 2.87 (app t, 4H), 3.85 (s, 3H), 4.01 (t, 2H, *J*= 6.0 Hz), 6.76 (td, 1H, *J*= 1.1 and 8.8 Hz), 6.92-6.96 (m, 4H), 7.01-7.07 (m, 3H), 7.12-7.18 (m, 1H), 7.21-7.25 (m, 2H), 7.56-7.61 (m, 2H), 7.78 (s, 1H), 7.85-7.89 (m, 2H), 8.10 (d, 1H, *J*= 6.9 Hz). ESI-MS *m/z* 533 $(M+H)^+$. ESI-MS/MS *m/z* 323 (100). Anal. ($C_{34}H_{36}N_4O_2$•2HCl•H_2O) C, H, N.

8-Chloro-7-[4-[4-[2-(4-methoxyphenyl)phenyl]piperazin-1-yl]butoxy]-4-methyl-2*H*-1-chromen-2-one (7f). Eluted with $CHCl_3$/MeOH (98:2, v/v). Pale yellow oil, 36% yield. ^1H NMR ($CDCl_3$): δ 1.65-1.72 (m, 2H), 1.85-1.94 (m, 2H,) 2.38-2.43 (m + d, 9H, *J*= 1.1 Hz), 2.85 (app t, 4H), 3.86 (s, 3H), 4.14 (t, 2H, *J*= 6.0 Hz), 6.17 (d, 1H, *J*= 1.1 Hz), 6.87-6.95 (m, 3H), 7.00-7.08 (m, 2H), 7.20-7.23 (m, 2H), 7.43 (d, 1H, *J*= 8.8 Hz), 7.55-7.60 (m, 2H). ESI-MS *m/z* 497 $(M+H)^+$. ESI-MS/MS *m/z* 497 (69), 335 (100). Anal. ($C_{31}H_{33}ClN_2O_4$•HCl•H_2O) C, H, N.

6-{2-[4-[2-(4-Methoxyphenyl)phenyll]piperazin-1-yl]butoxy}-2-methyl-2*H*-benzo[b][1,4]oxazin-3(4*H*)-one (7g). Eluted with $CHCl_3$/MeOH (95:5, v/v). Pale yellow oil, 65% yield. ^1H NMR ($CDCl_3$): δ 1.57 (d, 3H, *J*= 6.8 Hz), 1.61-1.67 (m, 2H), 1.75-1.80 (m, 2H,) 2.39 (app t, 6H), 2.87 (app t, 4H), 3.87 (s, 3H), 3.91 (t, 2H, *J*= 6.4 Hz), 4.57-4.61 (m, 1H), 6.35 (d, 1H, *J*= 2.4 Hz), 6.49 (dd, 1H, *J*= 2.4 and 8.8 Hz), 6.88 (d, 1H, *J*= 8.8 Hz), 6.93-6.95 (m, 2H), 7.02-7.08

(m, 2H), 7.22-7.27 (m, 2H), 7.58-7.60 (m, 2H), 8.07 (br s, 1H, D_2O exchanged). ESI-MS *m/z* 524 $(M+Na)^+$. ESI-MS/MS *m/z* 323 (100). Anal. ($C_{30}H_{35}N_2O_4$•HCl•H_2O) C, H, N.

1-[4-(4-Chloro-3-fluorophenoxy)but-2-ynyl]-4-[2-(4-methoxyphenyl)phenyl]piperazine (9). Eluted with $CHCl_3$/AcOEt (1:1, v/v). Pale yellow oil, 32% yield. ^1H NMR ($CDCl_3$): δ 2.45 (app t, 4H), 2.88 (app t, 4H), 3.26-3.28 (m, 2H), 3.84 (s, 3H), 4.69-4.70 (m, 2H), 6.72 (ddd, 1H, *J*= 2.7 and 7.7 Hz; J_{H-F}= 1.0 Hz), 6.80 (dd, 1H, *J*= 2.7 Hz; J_{H-F}= 10.7 Hz), 6.90-6.93 (m, 2H), 7.03-7.09 (m, 2H), 7.21-7.25 (m, 3H), 7.55-7.58 (m, 2H). ESI-MS *m/z* 487 $(M+H)^+$. ESI-MS/MS *m/z* 342 (100), 291 (91). Anal. ($C_{27}H_{26}ClFN_2O_2$•HCl) C, H, N.

2-[4-[4-[2-(4-Methoxyphenyl)phenyl]piperidin-1-yl]butoxy]pyrazine (15a). Eluted with $CHCl_3$/MeOH (98:2, v/v). Pale yellow oil, 20% yield. ^1H NMR ($CDCl_3$): δ δ 1.64-1.77 (m, 5H), 1.79-1.89 (m, 5H,), 2.38 (app t, 2H), 2.65-2.69 (m, 1H), 2.96-2.98 (m, 2H), 3.87 (s, 3H), 4.02 (t, 2H, *J*= 6.4 Hz), 6.92-6.96 (m, 2H), 7.01-7.07 (m, 2H), 7.20-7.24 (m, 2H), 7.55-7.59 (m, 2H), 8.04-8.06 (m, 1H), 8.08 (d, 1H, *J*= 3.0 Hz), 8.19 (d, 1H, *J*= 1.4 Hz). ESI-MS *m/z* 418 $(M+H)^+$. ESI-MS/MS *m/z* 322 (100). Anal. ($C_{26}H_{31}N_3O_2$•HCl•H_2O) C, H, N.

4-[3-[4-[2-(4-Methoxyphenyl)phenyl]piperidin-1-yl]butoxy]phenyl)imidazo[1,2-a]pyridine (15b). Eluted with $CHCl_3$/MeOH (98:2, v/v). Pale yellow oil, 30% yield. ^1H NMR ($CDCl_3$): δ 1.64-1.77 (m, 5H), 1.79-1.89 (m, 5H,), 2.38 (app t, 2H), 2.65-2.69 (m, 1H), 2.96-2.98 (m, 2H), 3.87 (s, 3H), 4.02 (t, 2H, *J*= 6.4 Hz), 6.75 (td, 1H, *J*= 1.2 and 7.0 Hz), 6.93-6.97 (m, 4H), 7.12-7.23 (m, 5H), 7.31 (td, 1H, *J*= 2.3 and 6.4 Hz), 7.37-7.40 (m, 1H), 7.59-7.62 (m, 1H), 7.77 (s, 1H), 7.85-7.88 (m, 2H), 8.10 (d, 1H, *J*= 7.0 Hz). ESI-MS *m/z* 532 $(M+H)^+$. ESI-MS/MS *m/z* 322 (100). Anal. ($C_{35}H_{37}N_3O_2$•HCl) C, H, N.

2-[5-[4-[2-(4-Methoxyphenyl)phenyl]piperazin-1-yl]-3,3-dimethylpentoxy]pyrazine (25).

Eluted with $CHCl_3$/MeOH (98:2, v/v). Pale yellow oil, 20% yield. ^1H NMR ($CDCl_3$): δ 0.91(s, 6H), 1.38-1.44 (m, 2H), 1.63-1.68 (m, 2H,) 2.26-2.31 (m, 6H), 2.80 (app t, 4H), 3.78 (s, 3H), 4.29 (t, 2H, *J*= 6.4 Hz), 6.84-6.89 (m, 2H), 6.94-7.00 (m, 2H), 7.13-7.23 (m, 2H), 7.49-7.52 (m, 2H), 7.99-8.00 (m, 1H), 8.02 (d, 1H, *J*= 3.0 Hz), 8.11 (d, 1H, *J*= 1.1 Hz). ESI-MS *m/z* 483 $(M+Na)^+$. ESI-MS/MS *m/z* 365 (100). Anal. ($C_{28}H_{36}N_4O_2$•HCl) C, H, N.

2-[5-[4-[2-(4-Methoxyphenyl)phenyl]piperazin-1-yl]-4,4-dimethylpentoxy]pyrazine (26).

Eluted with $CHCl_3$/MeOH (98:2, v/v). Pale yellow oil, 30% yield. ^1H NMR ($CDCl_3$): δ 0.91(s, 6H), 1.38-1.44 (m, 2H), 1.63-1.68 (m, 2H,), 2.38 (app t; 4H), 2.45 (t, 2H, *J*= 6.4 Hz), 2.80 (app t, 4H), 3.78 (s, 3H), 4.29 (t, 2H, *J*= 6.4 Hz), 6.84-6.89 (m, 2H), 6.94-7.00 (m, 2H), 7.13-7.23 (m, 2H), 7.49-7.52 (m, 2H), 7.99-8.00 (m, 1H), 8.02 (d, 1H, *J*= 3.0 Hz), 8.11 (d, 1H, *J*= 1.1 Hz). ESI-MS *m/z* 483 $(M+Na)^+$. ESI-MS/MS *m/z* 365 (100). Anal. ($C_{28}H_{36}N_4O_2$•HCl) C, H, N.

Radioligand Binding Assays

Materials. Cell culture reagents were purchased from EuroClone (Milan, Italy). G418 (geneticin), 5-HT, NAN-190 were obtained from Sigma-Aldrich (Milano, Italy). 5-CT was purchased from Tocris Bioscience (Bristol, UK). [^{3}H]-5-CT and [^{3}H]-8-OH-DPAT were obtained from PerkinElmer Life and Analytical Sciences (Boston, MA, USA). MultiScreen plates with Glass fiber filters was purchased from Merck Millipore (Billerica, MA, USA). pcDNA3.1(+) vector containing the target 5-HT_{1A} DNA sequence was purchased from cDNA Resource Center (Bloomsberg, PA, USA), FuGENE HD Transfection Reagent was obtained from Promega (Madison, Wisconsin, USA).

Cell culture. HEK-293 cell line was grown in DMEM high glucose supplemented with 10% fetal bovine serum, 2 mM glutamine, 100 U/mL penicillin, 100 μg/mL streptomycin, in a humidified incubator at 37 °C with a 5% CO_2 atmosphere. HEK-293-5HT_{7A} and HEK-293-5-HT_{1A} transfected cell lines were grown in DMEM high glucose supplemented with 10% fetal bovine serum, 2 mM

glutamine, 100 U/mL penicillin, 100 μg/mL streptomycin, 0.8 μg/mL G418, in a humidified incubator at 37 °C with a 5% CO_2 atmosphere.

HEK-293 Transfection with 5-HT$_{1A}$R [57]. To develop stably HEK-293-5-HT$_{1A}$ cell line, HEK-293 cells were plated at a density of 2×10^6 cells in growth medium in 100 mm Petri dishes and incubated at 37 °C overnight. Cells were transfected with 17 μg of the pcDNA3.1(+) vector containing the target 5-HT$_{1A}$R DNA sequence, as per standard protocol using FuGENE HD Transfection Reagent in Opti-MEM medium without serum. Vector-expressing cells were selected using geneticin (G418). After transfection, cells were placed in normal growth medium. After 1 day, cells were detached and re-plated into growth medium containing geneticin (0.8 mg/mL) and cultured for 20 days. Surviving cell clones were picked out and propagated separately in 60 mm Petri dishes in the same medium, with 0.8 mg/mL geneticin. To suppress reversion of the phenotype, all subsequent cell cultures were carried out in growth medium as described above, supplemented with 0.8 mg/mL geneticin.

Saturation binding assay at human cloned 5-HT$_{1A}$R. The saturation experiments were carried out as previously reported [57]. 5-HT$_{1A}$Rs were radiolabeled using [^{3}H]-8-OH-DPAT concentrations of 0.1–20 nM. Samples contained 100 μg HEK-293 5-HT$_{1A}$ membranes, radioligand and 10 μM NAN-190 to determine non-specific binding were incubated in a final volume of 0.5 mL (50 mM TRIS-HCl, pH 7.4, 4 mM $MgCl_2$, 0.1% ascorbic acid, 0.1 nM EDTA, 10 μM pargyline hydrochloride) for 60 min at 25 °C. The suspension was filtered through Whatman GF/C glass microfiber filters presoaked in 0.3% polyethylenimine (PEI) for at least 30 min prior to use. The filters were washed 3 × 1 mL ice-cold buffer (50 mM TRIS-HCl, pH 7.4). Scatchard parameters (K_d and B_{max}) were determined by nonlinear curve fitting, using the Prism, version 5.0, GraphPad software.

Radioligand binding at human cloned 5-HT$_{1A}$R. 5-HT$_{1A}$R binding was carried out as already reported [57]. The experiment was performed in MultiScreen plates (Merck Millipore) with Glass fiber filters (GF/C), presoaked in 0.3% PEI for 20 min. After this time, 100 μg of HEK-293-5-HT$_{1A}$

membranes, 1.5 nM [^{3}H]-8-OH-DPAT, the test compound was suspended in a 0.25 mL of incubation buffer (50 mM TRIS-HCl pH 7.4, 4 mM $MgCl_2$, 0.1% ascorbic acid, 0.1 nM EDTA, 10 μM pargyline hydrochloride). The samples were incubated for 60 min at 25 °C. The incubation was stopped by rapid filtration and the filters were washed with 3 × 0.25 mL of ice-cold buffer (50 mM TRIS-HCl, pH 7.4). Nonspecific binding was determined in the presence of 10 μM NAN-190. Approximately 90% of specific binding was determined under these conditions. Concentrations required to inhibit 50% of radioligand specific binding (IC_{50}) were determined by using six to nine different concentrations of the test compound in two or three experiments with samples in duplicate. Apparent inhibition constants (K_i) values was determined by nonlinear curve fitting, using the Prism, version 5.0, GraphPad software.

Radioligand binding at human cloned 5-HT$_7$Rs. 5-HT$_7$R binding was carried out as previously reported [57]. The experiment was performed in MultiScreen plates (Merck Millipore) with Glass fiber filters (GF/C), presoaked in 0.3% PEI for 20 min. After this time, 130 μg of HEK-293-5-HT$_{7A}$ membranes, 1 nM [^{3}H]-5-CT, the test compounds were suspended compound in 0.25 mL of incubation buffer (50 mM TRIS-HCl, pH 7.4, 4 mM $MgCl_2$, 0.1% ascorbic acid, 10 μM pargyline hydrochloride). The samples were incubated for 60 min at 37 °C. The incubation was stopped by rapid filtration and the filters were washed with 3 × 0.25 mL of ice-cold buffer (50 mM TRIS-HCl, pH 7.4). Nonspecific binding was determined in the presence of 10 mM 5-CT. Approximately 90% of specific binding was determined under these conditions. Concentrations required to inhibit 50% of radioligand specific binding (IC_{50}) were determined by using six to nine different concentrations of the drug studied in two or three experiments with samples in duplicate. Apparent inhibition constants (K_i) values was determined by nonlinear curve fitting, using the Prism, version 5.0, GraphPad software.

Stability Assays in Rat Liver Microsomes

Test compounds were pre-incubated at 37 °C with rat liver microsomes (Tebu-Bio, Milan, Italy) (1.0 mg/mL microsomal protein) at 10 μM final concentration in 100 mM potassium phosphate buffer (pH 7.4) for 10 min. Metabolic reactions were initiated by the addition of the NADPH regenerating system (containing 10 mM NADP, 50 mM glucose-6-phosphate, and 10 unit/mL glucose-6-phosphate dehydrogenase, final glucose-6-phosphate dehydrogenase concentration, 1 unit/mL). Aliquots were removed at specific time endpoints and immediately mixed with an equal volume of cold acetonitrile containing the internal standard. Test compound incubated with microsomes without NADPH regenerating system was included. Quenched samples were centrifuged at 4500 rpm for 15 min and the supernatants were injected for quantification analysis. Samples (100 μL) were analyzed by using an Agilent 1260 Infinity Binary LC System equipped with a diode array detector (Open Lab software was used to analyze the chromatographic data) and a Phenomenex Gemini C-18 column (250 x 4.6 mm, 5 μm particle size). The samples were eluted using CH_3CN/20 mM ammonium formate pH 5.5 (7:3, v/v) as eluent (volumetric flow rate =1 mL/min). Concentrations were quantified by measuring the area under the peak.

The percentage of the parent compound remaining after a 30-min incubation has been calculated according to the equation:

$$\% \text{ of parent compound remaining after 30 min} = C_{parent}/C_{control} \cdot 100$$

where C_{parent} is ligand concentration after incubation with microsome fraction and NADPH regenerating system and $C_{control}$ is ligand concentration after incubation with microsome fraction only.

The *in vitro* half-life ($t_{1/2}$) was calculated using the expression $t_{1/2}=0.693/b$, where *b* is the slope found in the linear fit of the natural logarithm of the fraction remaining of the parent compound vs incubation time [37]. *In vitro* half-life was then used to calculate the intrinsic plasma clearance (CL_{int}) according to the following equation:

$$CL_{int} = \frac{0.693}{\text{in vitro } t_{1/2}} \cdot \frac{1}{\text{mg/mL microsomal protein}}$$

Stability Assays in Rat Hepatocytes

Pooled cryopreserved rat hepatocytes were purchase from XenoTech (Tebu-bio, Milan, Italy). The rat hepatocytes were thawed and re-suspended in the incubation medium (Hepatocytes Incubation Media, cat# K2500, containing Waymouth's Media - pH 7.4 supplemented with fetal bovine serum, insulin, dexamethasone, sodium pyruvate, L-glutamine) according to manufacturer's instructions. The cells were counted using the Trypan Blue exclusion method. The cells were seeded in a 96-well Bio-Coat™ Collagen I Cellware (Corning, Turin, Italy) at a final concentration of $6 \cdot 10^4$ cells/well. The final incubation contained 10 μM of tested compound in a final volume of 200 μL. The incubation was carried out at 37 °C. At various time points (0, 3, 10, 30, 60, 120 min), reactions were quenched adding an equal volume of cold acetonitrile containing the internal standard. The samples were centrifuged at 3000 rpm for 10 min at 4 °C. The supernatants were injected for quantification analysis. Samples (100 μL) were analyzed by using an Agilent 1260 Infinity Binary LC System equipped with a diode array detector (Open Lab software was used to analyze the chromatographic data) and a Phenomenex Gemini C-18 column (250 × 4.6 mm, 5 μm particle size). The samples were eluted using CH_3CN/20 mM ammonium formate pH 5.5 (7:3, v/v), at a volumetric flow rate = 1 mL/min. Concentrations were quantified by measuring the area under the peak. Risperidone was included as reference compound (half-life= 68 min; $CL_{int,\ scaled}$= 12.1 mL/min/kg).

The *in vitro* half-life ($t_{1/2}$) was calculated using the expression $t_{1/2}=0.693/b$, where b is the slope found in the linear fit of the natural logarithm of the fraction remaining of the parent compound vs incubation time [37]. *In vitro* half-life was then used to calculate the intrinsic plasma clearance (CL_{int}) according to the following equation:

$$CL_{int,\ app} = \frac{0.693}{\text{in vitro } t_{1/2}} \cdot \frac{\text{mL incubation}}{6 \cdot 10^4 \text{ cells}} \cdot \frac{1000\ \mu\text{L}}{\text{mL}}$$

Plasma Proteins Binding Assay

The determination of compounds binding to plasma proteins was performed by incubating a fixed concentration of the compound with different concentrations of immobilized human serum albumin (HSA) and human α1-acid glycoprotein (AGP), using the TRANSIL^{XL} PPB Binding Kit (TMP-0212-2096, Sovicell, Leipzig, Germany). An 8-well unit of the TRANSIL assay plate was used for each compound, where six wells contain increasing concentrations of HSA and AGP immobilized on silica beads suspended in PBS at pH 7.4, and two wells contain buffer only and serve as references to account for non-specific binding.

The TRANSIL assay plate was thawed for 3 h at room temperature and centrifuged at 750*g* for 5 s. Then, 15 µL of an 80 µM stock solution of the compound in PBS (final concentration was 5 µM) were added to each well of the 8-well unit, and the plate was incubated in a plate shaker at 1000 rpm for 12 min at room temperature. After this time, the plate was centrifuged at 750*g* for 10 min, and 50 µL of the supernatants were transfer for analytical quantification by UV-HPLC. Samples were analyzed by using an Agilent 1260 Infinity Binary LC System equipped with a diode array detector (Open Lab software was used to analyze the chromatographic data) and a Phenomenex Gemini C-18 column (250 × 4.6 mm, 5 µm particle size). The samples were eluted using CH_3CN/20 mM ammonium formate pH 5.5 (7:3, v/v), at a volumetric flow rate = 1 mL/min.

The binding percentage was calculated from the remaining free compound concentration in the supernatant of each well, using the spreadsheet and algorithms supplied with the kit.

Profiling on hERG Channel

Compound profiling performed by Axxam S.p.A. (Milan, Italy) on hERG-CHO cells using an automated patch-clamp protocol.

Cell culture conditions. CHO-K1/hERG DUO (Sophion-Biolin) cells were cultured in HAM'S F-12 (BioWhittaker cat. BE12- 615F) supplemented with 100× Penicillin/Streptomycin (BioWhittaker cat. DE17-602E, final concentration 1%), 50 mg/mL of G418 (Sigma cat. G8168-100mL; final

concentration 100 μg/mL), 100 mg/mL of Hygromycin B (InvivoGen cat. ant-hm-1; final concentration 100 μg/mL) and Fetal Bovine Serum (Sigma cat. F7524; final concentration 10%). Standard propagation conditions consist in plating 0.8 – 1×106 cells in T225 flasks (twice a week).

Cell preparation. 72 hours before experiment, 0.8 million cells were seeded onto T225. Just before the experiments, cells were washed twice with D-PBS w/o Ca^{2+}/Mg^{2+} (Euroclone cat. ECB4004L) and detached from the flask with trypsin-EDTA (Sigma cat. T4174, diluted 1:10 v/v). Cells were then re-suspended in the suspension solution: 25 mL EX-CELL ACF CHO medium (Sigma cat. C5467); 0.625 mL HEPES (Lonza cat. BE17-737E); 0.25 mL of 100x Penicillin/Streptomycin (LONZA cat. DE17-602E), 0.1 mL of Soybean trypsin inhibitor 10 mg/mL (Sigma cat. T6522) and placed on the automated patch-clamp instrument QPatch 16X (Sophion, Denmark).

Test compound solution preparation and storage. A 10 μM stock solution of test compounds was prepared in DMSO and stored at -20 °C in aliquots. The intracellular solution contains (mM) 120 KCl, 5.374 $CaCl_2$, 1.75 $MgCl_2$, 10 EGTA, 10 HEPES, 4 sodium-ATP (pH 7.2 with KOH). The extracellular solution contains (mM): 145 NaCl, 4 KCl, 1 $MgCl_2$, 2 $CaCl_2$, 10 HEPES, 10 glucose (pH 7.4 with NaOH).

Data acquisition and pulse protocols. Standard whole-cell voltage clamp experiments were performed at room temperature. For data acquisition the Sophion-Biolin software (Axxam S.p.A., Milan) was used. For voltage clamp experiments on IhERG, data are sampled at 5 KHz. Cells are held at -90 mV and the hERG current is evoked using the following voltage protocol: 200 ms step at -50 mV; 2000 ms step at +20 mV; 2000 ms step at -50 mV; 100 ms step at 0 mV, applied every 15 seconds.

Data analysis. For data collection, the Sophion-Biolin software was used and the analysis was performed off-line using Excel and GraphPad Prism (v. 6.02). The dose-response curves data were fitted with the following equation:

$$Y = 100/(1+10\text{^}((\text{Log}IC_{50}\text{-}X)*\text{Hill Slope}))$$

where: X = log of concentration; Y = normalized response, 100% down to 0%, decreasing as X increases; $LogIC_{50}$ = same log units as X; Hill Slope = slope factor or Hill slope, unitless.

Recording of voltage-gated hNav1.5 sodium currents

Compounds **1e**, **7g**, and **14e** were tested on the human cardiac sodium channel, as previously described [58]. The calcium-phosphate co-precipitation method was used to obtain transient transfection of HEK293T cells. Briefly, HEK293T cells were incubated for 24 hours with 100 ng/mL of the pRc-CMV plasmid containing the full-length cDNA encoding the α-subunit of the human cardiac hNav1.5 sodium channel, and 50 ng/mL of a plasmid expressing the CD8 receptor and the auxiliary human voltage-gated sodium channel β1 subunit (pCD8-IRES-hβ1). Patch-clamp experiments were performed 48−72 h after transfection on cells marked with anti-CD8 antibody-coated microbeads (Dynal-Invitrogen, Milan, Italy). The whole-cell sodium currents were recorded at room temperature (20−22 °C) using Axopatch-1D amplifier (Axon Instruments Inc., Union City, CA, USA) and pClamp software (Axon Instruments). The composition of the bath solution was (mM): 150 NaCl, 4 KCl, 2 $CaCl_2$, 1 $MgCl_2$, 5 HEPES and 5 glucose (pH 7.4). The pipette solution contained (mM): 120 CsF, 10 CsCl, 10 NaCl, 5 EGTA, and 5 HEPES (pH 7.2). In these conditions, the pipette resistance ranged between 2 and 4 MΩ. The patched cell was exposed to a gravity-driven stream of bath solution. Sodium currents were elicited by a 25 ms-long test pulse to -30 mV from a holding potential of −120 mV applied at 0.1, 2, and 10 Hz frequencies, first in control bath solution then in bath solution supplemented with 100 μM drug.

Patch clamp on brain slices

All animal experimentation was conducted in accordance with the European Community Council guidelines (2010/63/EU) and was approved by the University Institutional Animal Care and Use Committee (Projects # 181; 250 – approval number: 352/2016-PR). Experiments were performed on wild-type mice from C57BL/6J strain. Mice were maintained in the animal facility of Catania

University with a controlled temperature (21 ± 1 °C) and humidity (50%) on a 12 h light/dark cycle, with ad libitum food and water.

Electrophysiology. Acute hippocampal slices were prepared as previously described [47] from WT mice on a C57BL/6J background (source: Envigo RMS Srl, Italy). A total number of 11 animals was used (6 males and 5 females) at a postnatal (PN) age of 11-15 days. The brains were removed, placed in oxygenated ice-cold artificial cerebrospinal fluid (ACSF; in mM NaCl 124; KCl 3.0; NaH_2PO_4 1.2; $MgSO_4$ 1.2; $CaCl_2$ 2.0; $NaHCO_3$ 26; D-glucose 10, pH 7.3) and cut into 300 µm slices with a vibratome (Leica VT 1200S). Slices were continually perfused with oxygenated ACSF and viewed with infrared microscopy (Leica DMLFS). Schaffer collaterals were stimulated with negative current pulses (duration 0.3 ms, delivered every 15 s by A310 Accupulser, WPI, USA). Evoked excitatory post synaptic currents (EPSCs) were recorded under whole-cell from CA1 pyramidal neurons (holding potential -70 mV; EPC7-plus amplifier HEKA, Germany). Stimulation intensity was set to induce half-maximal EPSC amplitude. Series resistance (Rs) was continuously monitored by 10 mV hyperpolarizing pulses; recordings were discarded from analysis if Rs changed by more than 20%. EPSC traces were filtered at 3 kHz and digitized at 10 kHz. Data were acquired and analyzed using Signal software (CED, England). The recording micropipette (resistance 1.5-3 MΩ) was filled with intracellular solution (in mM: K-gluconate 140; HEPES 10; NaCl 10; $MgCl_2$ 2; EGTA 0.2; Mg-ATP 3.5; Na-GTP 1; pH 7.3).

To isolate AMPA receptor-mediated EPSCs, bath solution (ACSF; flow rate of 1.5 mL/min) routinely contained (-)-bicuculline methiodide (5 µM, Hello Bio) and D-(-)-2-amino-5-phosphonopentanoic acid (D-AP5, 50 µM, Hello Bio). S-3,5-DHPG (100 µM; Hello Bio), **1e** (100 nM) and **7g** (100 nM) were dissolved in ACSF and applied by bath perfusion.

For LTD data analysis, peak amplitude values of EPSCs were averaged over 1 min and expressed as % of baseline EPSC amplitude (calculated from EPSCs recorded during at least 15 min before DHPG application). % EPSC values from groups of neurons were pooled (mean ± standard error of mean, SEM) and graphically represented as a function of time. The amount of mGluR-LTD was

calculated 40 min after LTD induction and was expressed as percentage of baseline (% EPSC amplitude; mean ± SEM from all tested neurons). EPSC amplitude values from two groups of neurons were compared using the Student's t-test, with n indicating the number of neurons tested in each condition (GraphPad Prism 6, U.S.A.).

Behavioral Testing

Research involving animals have been performed in accordance with NIH guidelines and protocols approved by the Animal Care Committee of the University of Illinois at Chicago. The nesting removal experiment was conducted in male and female WT and KO mice. Experiments were conducted on littermate KO and WT mice bred in the laboratory from congenic C57BL/6J stock obtained from Jackson Laboratories (Bar Harbor, ME, USA). KO and WT mice (12-16 weeks old) used for testing were obtained from heterozygous *Fmr1*-KO dams mated with either WT or hemizygous *Fmr1*-KO sires. Mice were genotyped by PCR of DNA from tail snips (Transnetyx, Cordova, TN, USA).

Mice were paired housed with a same sex littermate throughout the duration of the experimental period. There was an equal number of female (n = 4) and male (n = 4) mice in the WT and KO groups tested. Each mouse was tested twice. Once following a vehicle (5% dimethyl sulfoxide in sterile saline) injection and once following an injection of **7g** (3 mg/kg). Tests occurred one week apart, and treatments were counterbalanced across mice. Twenty-minutes prior to behavioral testing, a mouse received an intraperitoneal injection of either vehicle or **7g**. After 20 minutes, a mouse was placed in a standard hold cage (28 × 19 × 12.5 cm) that contained new bedding (Teklad Sani-chips 7090, Envigo, Indianopolis, IN, USA) that was 5 cm deep with approximately 4 grams of nesting material (Crinkle Nest Kraft #22, Animal Feeds & Needs, Arlington Heights, IL, USA) placed on top of the bedding. The nesting material was left in the cage for 10 minutes. The time spent digging was measured with the nesting in the cage by an experimenter. Digging was defined as repetitive movements of forelimbs or hindlimbs that displace the bedding. After 10 minutes

elapsed, the nesting material was removed from the test cage. Time spent digging was again measured for a 10-minute period. For both nesting in and nesting out condition, the time spent digging was calculated by an experimenter blind to the genotype and treatment. In addition to digging behavior, locomotor activity was measured during the nesting out condition using Any-Maze software (Stoelting Inc., Wood Dale, IL, USA).

For digging behavior, a three-way analysis of variance (ANOVA) with repeated measures was conducted using treatment and genotype as between factors and nesting condition as the repeated measure. To analyze locomotor activity (distance traveled), a two-way ANOVA was employed using treatment and genotype as between factors. Significant interactions were followed up with Tukey's post-hoc tests.

APPENDIX A. SUPPLEMENTARY DATA

Elemental Analysis; RP-HPLC traces

FUNDING SOURCES

The present work was supported by Telethon Foundation Grant GGP13145 (Lucia Ciranna, Marcello Leopoldo) and in part by NIH grant HD084209 (Michael E. Ragozzino).

The authors declare no competing financial interest.

Authors Contribution

The manuscript was written through contributions of all authors. All authors have given approval to the final version of the manuscript.

Author Information

ORCID

Enza Lacivita: 0000-0003-2443-1174

Mauro Niso: 0000-0002-2846-1744

Lara Costa: 0000-0002-2465-8080

Michael E. Ragozzino: 0000-0001-6964-7046

Lucia Ciranna: 0000-0003-0274-6095

Marcello Leopoldo: 0000-0001-8401-2815

REFERENCES

[1] M. Leopoldo, E. Lacivita, F. Berardi, R. Perrone, P.B. Hedlund, Serotonin 5-HT7 receptor agents: Structure-activity relationships and potential therapeutic applications in central nervous system disorders. Pharmacol. Ther. 129 (2011) 120–148.

[2] M.N. Modica, E. Lacivita, S. Intagliata, L. Salerno, G. Romeo, V. Pittalà, M. Leopoldo, Structure-activity relationships and therapeutic potentials of 5-HT_7 receptor ligands: an update. J. Med. Chem. 61 (2018) 8475–8503.

[3] P.B. Hedlund, The 5-HT_7 receptor and disorders of the nervous system: an overview. Psychopharmacology (Berl) 206 (2009) 345–354.

[4] E. Kvachnina, G. Liu, A. Dityatev, U. Renner, A. Dumuis, D.W. Richter, G. Dityateva, M. Schachner, T.A. Voyno-Yasenetskaya, E.G. Ponimaskin, 5-HT7 receptor is coupled to G alpha subunits of heterotrimeric G12-protein to regulate gene transcription and neuronal morphology. J. Neurosci. 25 (2005) 7821–7830.

[5] F. Kobe, D. Guseva, T.P. Jensen, A. Wirth, U. Renner, D. Hess, M. Muller, L. Medrihan, W. Zhang, M. Zhang, K. Braun, S. Westerholz, A. Herzog, K. Radyushkin, A. El-Kordi, H. Ehrenreich, D.W. Richter, D.A. Rusakov, E Ponimaskin, 5-HT7R/G12 signaling regulates neuronal morphology and function in an age-dependent manner. J. Neurosci. 32 (2012) 2915–2930.

[6] L. Speranza, J. Labus, F. Volpicelli, D. Guseva, E. Lacivita, M. Leopoldo, G.C. Bellenchi, U. di Porzio, M. Bijata, C. Perrone-Capano, E. Ponimaskin, Serotonin 5-HT7 receptor increases the

density of dendritic spines and facilitates synaptogenesis in forebrain neurons. J. Neurochem. 141 (2017) 647–661.

[7] F. Volpicelli, L. Speranza, S. Pulcrano, R. De Gregorio, M. Crispino, C. De Sanctis, M. Leopoldo, E. Lacivita, U. di Porzio, G.C. Bellenchi, C. Perrone-Capano, The microRNA-29a modulates serotonin 5-HT_7 receptor expression and its effects on hippocampal neuronal morphology. Mol. Neurobiol. 56 (2019) 8617–8627.

[8] L. Speranza, A. Chambery, M. Di Domenico, M. Crispino, V. Severino, F. Volpicelli, M. Leopoldo, G.C. Bellenchi, U. di Porzio, C. Perrone-Capano, The serotonin receptor 7 promotes neurite outgrowth via ERK and Cdk5 signaling pathways. Neuropharmacology 67 (2013) 155–167.

[9] L. Speranza, T. Giuliano, F. Volpicelli, M.E. De Stefano, L. Lombardi, A. Chambery, E. Lacivita, M. Leopoldo, G.C.; Bellenchi, U. di Porzio, M. Crispino, C. Perrone-Capano, Activation of 5-HT7 receptor stimulates neurite elongation through mTOR, Cdc42 and actin filaments dynamics. Front. Behav. Neurosci. 9 (2015) 62.

[10] T.R.; Stankiewicz, D.A. Linseman, Rho family GTPases: key players in neuronal development, neuronal survival, and neurodegeneration. Front. Cell. Neurosci. 8 (2014) 314.

[11] P. Di Pilato, M. Niso, W. Adriani, E. Romano, D. Travaglini, F. Berardi, N.A. Colabufo, R. Perrone, G. Laviola, E. Lacivita, M. Leopoldo, Selective agonists for serotonin 7 (5-HT7) receptor and their applications in preclinical models: an overview. Rev. Neurosci. 25 (2014) 401–415.

[12] L. Costa, M. Spatuzza, S. D'Antoni, C.M. Bonaccorso, C. Trovato, S.A. Musumeci, M. Leopoldo, E. Lacivita, M.V. Catania, L. Ciranna, Activation of 5-HT7 serotonin receptors reverses metabotropic glutamate receptor-mediated synaptic plasticity in wild-type and Fmr1 knockout mice, a model of Fragile X syndrome. Biol Psychiatry 72 (2012) 924–933.

[13] L. Costa, L.M. Sardone, E. Lacivita, M. Leopoldo, L. Ciranna, Novel agonists for serotonin 5-HT7 receptors reverse metabotropic glutamate receptor-mediated long-term depression in the hippocampus of wild-type and Fmr1 KO mice, a model of Fragile X Syndrome. Front Behav Neurosci 9 (2015) 65.

[14] K.M. Huber, S.M. Gallagher, S.T. Warren, M.F. Bear, Altered synaptic plasticity in a mouse model of fragile X mental retardation. Proc. Natl. Acad. Sci. U.S.A, 99 (20) 27746–27750.

[15] L. Costa, L.M. Sardone, C.M.; Bonaccorso, S. D'Antoni, M. Spatuzza, W. Gulisano, M.R. Tropea, D. Puzzo, M. Leopoldo, E. Lacivita, M.V. Catania, L. Ciranna, Activation of serotonin 5-HT_7 receptors modulates hippocampal synaptic plasticity by stimulation of adenylate cyclases and rescues learning and behavior in a mouse model of Fragile X syndrome. Front. Mol. Neurosci. 11 (2018) 353.

[16] B. De Filippis, P. Nativio, A. Fabbri, L. Ricceri, W. Adriani, E. Lacivita, M. Leopoldo, F. Passarelli, A. Fuso, G. Laviola, Pharmacological stimulation of the brain serotonin receptor 7 as a novel therapeutic approach for Rett syndrome. Neuropsychopharmacology 39 (2014) 2506–2518.

[17] B. De Filippis, V. Chiodi, W. Adriani, E. Lacivita, C. Mallozzi, M. Leopoldo, M. R. Domenici, A. Fuso, G. Laviola, Long-lasting beneficial effects of central serotonin receptor 7 stimulation in female mice modeling Rett syndrome. Front. Behav. Neurosci 9 (2015) 86.

[18] D. Valenti, L. de Bari, D. Vigli, E. Lacivita, M. Leopoldo, G. Laviola, R.A. Vacca, B. De Filippis, Stimulation of the brain serotonin receptor 7 rescues mitochondrial dysfunction in female mice from two models of Rett syndrome. Neuropharmacology 121 (2017) 79–88.

[19] D. Vigli, L. Rusconi, D. Valenti, P. La Montanara, L. Cosentino, E. Lacivita, M. Leopoldo, E. Amendola, C. Gross, N. Landsberger, G. Laviola, C. Kilstrup-Nielsen, R.A. Vacca, B. De Filippis, Rescue of prepulse inhibition deficit and brain mitochondrial dysfunction by pharmacological stimulation of the central serotonin receptor 7 in a mouse model of CDKL5 Deficiency Disorder. Neuropharmacology. 144 (2019) 104–114.

[20] L. Ciranna, M.V. Catania, 5-HT7 receptors as modulators of neuronal excitability, synaptic transmission and plasticity: physiological role and possible implications in autism spectrum disorders. Front. Cell. Neurosci. 8 (2014) 250.

[21] E. Lacivita, R. Perrone, L. Margari, M. Leopoldo, Targets for drug therapy for autism spectrum disorder: challenges and future directions. J. Med. Chem. 60 (2017) 9114–9141.

[22] A.S. Hogendorf, A. Hogendorf, K. Popiołek-Barczyk, A. Ciechanowska, J. Mika, G. Satała, M. Walczak, G. Latacz, J. Handzlik, K. Kieć-Kononowicz, E. Ponimaskin, S. Schade, A. Zeug, M. Bijata, M. Kubicki, R. Kurczab, T. Lenda, J. Staroń, R. Bugno, B. Duszyńska, B. Pilarski, A.J. Bojarski, Fluorinated indole-imidazole conjugates: selective orally bioavailable 5-HT_7 receptor low-basicity agonists, potential neuropathic painkillers. Eur. J. Med. Chem. 170 (2019) 261–275.

[23] R.D. Taylor, M. MacCoss, A.D. Lawson, Combining molecular scaffolds from FDA approved drugs: application to drug discovery. J. Med. Chem. 60 (2017) 1638–1647.

[24] H.D. Hansen, E. Lacivita, P. Di Pilato, M.M. Herth, S. Lehel, A. Ettrup, V.L. Andersen, A. Dyssegaard, P. De Giorgio, R. Perrone, F. Berardi, N.A. Colabufo, M. Niso, G.M. Knudsen, M. Leopoldo, Synthesis, radiolabeling and in vivo evaluation of [^{11}C](R)-1-[4-[2-(4-methoxyphenyl)phenyl]piperazin-1-yl]-3-(2-pyrazinyloxy)-2-propanol, a potential PET radioligand for the 5-HT_7 receptor. Eur. J. Med. Chem. 79 (2014) 152–163.

[25] R.D.E. Sewell, R.A. Glennon, M. Dukat, H. Stark, E. Schunack, P.G. Strange, Neurotransmitters, Agonists and Antagonists. In Smith and Williams' Introduction to the Principles of Drug Design and Action, 3rd ed.; Smith, H. J., Williams, H., Eds.; CRC Press, (1998) pp 387–433.

[26] M. Leopoldo, E. Lacivita, M. Contino, N.A. Colabufo, F. Berardi, R. Perrone, Structure-activity relationship study on N-(1,2,3,4-tetrahydronaphthalen-1-yl)-4-aryl-1-piperazinehexanamides, a class of 5-HT_7 receptor agents. 2. J. Med. Chem. 50 (2007) 4214–4221.

[27] M. Leopoldo, E. Lacivita, P. De Giorgio, C. Fracasso, S. Guzzetti, S. Caccia, M. Contino, N.A. Colabufo, F. Berardi, R. Perrone, Structural modifications of *N*-(1,2,3,4-tetrahydronaphthalen-1-yl)-4-aryl-1-piperazinehexanamides: influence on lipophilicity and 5-HT_7 receptor activity. Part III. J. Med. Chem. 51 (2008) 5813–5822.

[28] E. Lacivita, P. De Giorgio, D. Patarnello, M. Niso, N.A. Colabufo, F. Berardi, R. Perrone, G. Satala, B. Duszynska, A.J. Bojarski, M. Leopoldo, Towards metabolically stable 5-HT7 receptor

ligands: a study on 1-arylpiperazine derivatives and related isosters. Exp. Brain Res. 230 (2013) 569–582.

[29] Y. Shimokawa, H. Akiyama, E. Kashiyama, T. Koga, G. Miyamoto, High performance liquid chromatographic methods for the determination of aripiprazole with ultraviolet detection in rat plasma and brain: application to the pharmacokinetic study, J. Chromatogr. B Anal. Technol. Biomed. Life Sci. 821 (2005) 8e14.

[30] N.A. Meanwell, Fluorine and Fluorinated Motifs in the Design and Application of Bioisosteres for Drug Design. J. Med. Chem. 61 (2018) 5822–5880.

[31] M. Leopoldo, E. Lacivita, E. Passafiume, M. Contino, N.A. Colabufo, F. Berardi, R. Perrone, 4-[omega-[4-arylpiperazin-1-yl]alkoxy]phenyl)imidazo[1,2-a]pyridine derivatives: fluorescent high-affinity dopamine D3 receptor ligands as potential probes for receptor visualization. J. Med. Chem. 50 (2007) 50435047.

[32] Y. Chen, S. Wang, X. Xu, X. Liu, M. Yu, S. Zhao, S. Liu, Y. Qiu, T. Zhang, B.F. Liu, G. Zhang, Synthesis and biological investigation of coumarin piperazine (piperidine) derivatives as potential multireceptor atypical antipsychotics. J. Med. Chem. 56 (2013) 4671–4690.

[33] M. Cantillon, R. Ings, A. Prakash, L. Bhat, A population pharmacokinetic and pharmacodynamic analysis of RP5063 Phase 2 study data in patients with schizophrenia or schizoaffective disorder. Eur. J. Drug Metab. Pharmacokinet. 43 (2018) 573–585.

[34] R.A. Medina, J. Sallander, B. Benhamú, E. Porras, M. Campillo, L. Pardo, M.L. López-Rodríguez, Synthesis of new serotonin 5-HT_7 receptor ligands. Determinants of 5-HT_7/5-HT_{1A} receptor selectivity. J. Med. Chem. 52 (2009) 2384–2392.

[35] R.S. Obach, J.G. Baxter, T.E. Liston, B.M. Silber, B.C. Jones, F. MacIntyre, D.J. Rance, P. Wastall, The prediction of human pharmacokinetic parameters from preclinical and in vitro metabolism data. J. Pharmacol. Exp. Ther. 283 (1997) 46–48.

[36] E. Lacivita, S. Podlewska, L. Speranza, M. Niso, G. Satala, R. Perrone, C. Perrone-Capano, A. J. Bojarski, M. Leopoldo, Structural modifications of the serotonin 5-HT7 receptor agonist N-(4-

cyanophenylmethyl)-4-(2-biphenyl)-1-piperazinehexanamide (LP-211) to improve in vitro microsomal stability: A case study. Eur. J. Med. Chem. 120 (2016) 363–379.

[37] P. Chao, A.S. Uss, K.C. Cheng, Use of intrinsic clearance for prediction of human hepatic clearance. Expert Opin. Drug Metab. Toxicol. 6 (2010) 189–198.

[38] C.A. McNaney, D.M. Drexler, S.Y. Hnatyshyn, T.A. Zvyaga, J.O. Knipe, J.V. Belcastro M. Sanders, An automated liquid chromatography-mass spectrometry process to determine metabolic stability half-life and intrinsic clearance of drug candidates by substrate depletion, ASSAY Drug Dev. Technol. 6 (2008) 121–129.

[38] L. Di, C. Keefer, D.O. Scott, T.J. Strelevitz, G. Chang, Y.A. Bi, Y. Lai, J. Duckwoth, K. Fenner, M.D. Troutman, R.S. Obach, Mechanistic insights from comparing intrinsic clearance values between human liver microsomes and hepatocytes to guide drug design. Eur. J. Med. Chem. 57 (2012) 441–448.

[40] K.R. Lee, Y.J. Chae, T.S. Koo, Pharmacokinetics of lurasidone, a novel atypical anti-psychotic drug, in rats. Xenobiotica 41 (2011) 1100–1107.

[41] T. Swainston Harrison, C.M. Perry, Aripiprazole: a review of its use in schizophrenia and schizoaffective disorder. Drugs 64 (2004) 1715–1736.

[42] G. Eisenbrand, B. Pool-Zobel, V. Baker, M. Balls, B.J. Blaauboer, A. Boobis, A. Carere, S. Kevekordes, J.-C. Lhuguenot, R. Pieters, J Kleiner, Methods of in vitro toxicology. Food Chem. Toxicol. 40 (2002) 193–236.

[43] M. Mannerström, T. Toimela, T. Ylikomi, H. Tähti, The combined use of human neural and liver cell lines and mouse hepatocytes improves the predictability of the neurotoxicity of selected drugs. Toxicol. Lett. 165 (2006) 195–202.

[44] T. Sato, H. Yuki, K. Ogura, T. Honma, Construction of an integrated database for hERG blocking small molecules. PLoS One 13 (2018) e0199348.

[45] W. J. Jr Crumb, J. Vicente, L. Johannesen, D.G. Strauss, An evaluation of 30 clinical drugs against the comprehensive in vitro proarrhythmia assay (CiPA) proposed ion channel panel. J. Pharmacol. Toxicol. Methods 81 (2016) 251–262.

[46] M. De Bellis, R. Carbonara, J. Roussel, A. Farinato, A. Massari, S. Pierno, M. Muraglia, F. Corbo, C. Franchini, M.R. Carratù, A. De Luca, D. Conte Camerino, J.F. Desaphy, Increased sodium channel use-dependent inhibition by a new potent analogue of tocainide greatly enhances in vivo antimyotonic activity. Neuropharmacology 113 (2016) 206–216.

[47] L. Costa, C. Trovato, S.A. Musumeci, M.V. Catania, L. Ciranna, 5-HT_{1A} and 5-HT_7 receptors differently modulate AMPA receptor-mediated hippocampal synaptic transmission. Hippocampus 22 (2012) 790-801.

[48] C. Nicolaidis, C.C. Kripke, D. Raymaker, Primary care for adults on the autism spectrum. Med. Clin. North. Am. 98 (2014) 1169–1191.

[49] M. Prior, M.B. Macmillan, Maintenance of sameness in children with Kanner's syndrome. J. Autism Child. Schizophr. 3 (1973) 154–167.

[50] J.S. Silvestre, J.R. Prous, Comparative evaluation of hERG potassium channel blockade by antipsychotics. Methods Find. Exp. Clin. Pharmacol. 29 (2007) 457–465.

[51] J.W. Brown, A.R. Gangloff, A.J Jennings, P.H. Vu, Poly (ADP-Ribose) Polymerase (PARP) inhibitors (2010) WO2010/111626.

[52] S. Wagner, M.P. Law, B.; Riemann, V.W. Pike, H.-J. Breyholz, C. Hoeltke, A. Faust, O. Schober, M. Schaefers, K. Kopka, Synthesis of an ^{18}F-labelled high affinity β1-adrenoceptor PET radioligand based on ICI 89,406. J. Label. Compd. Radiopharm. 48 (2005) 721–733.

[53] Y. Kim, J. Kim, J. Tae, B.L. Roth, H. Rhim, G. Keum, G. Nam, H. Choo, Discovery of aryl-biphenyl-2-ylmethylpiperazines as novel scaffolds for 5-HT_7 ligands and role of the aromatic substituents in binding to the target receptor. Bioorg. Med. Chem. 21 (2013) 2568–2576.

[54] A.M. Equi, A.M. Brown, A. Cooper, S.K. Her, A.B. Watson, D.J. Robins, Oxidation of putrescine and cadaverine derivatives by diamine oxidases. Tetrahedron 47 (1991) 507– 518.

[55] T.F.J. Lampe, H.M.R. Hoffmann, Asymmetric synthesis of the C(10)-C(16) segment of the bryostatins. Tetrahedron Lett. 37 (1996) 7695–7698.

[56] J. Davis, R. Benhaddou, O. Fedoryak, R. Granet, P. Krausz, C. Bliard, M. De Monte, A.M. Aubertin, Potential antiviral agents. Part II. Synthesis and antiviral evaluation of pyrazinones substituted with acyclic chains. Nucleosides Nucleotides 17 (1998) 1489–1504.

[57] E. Lacivita, M. Niso, H.D. Hansen, P. Di Pilato, M.M.; Herth, S. Lehel, A. Ettrup, L. Montenegro, R. Perrone, F. Berardi, N.A. Colabufo, M. Leopoldo, G.M. Knudsen, Design, synthesis, radiolabeling and in vivo evaluation of potential positron emission tomography (PET) radioligands for brain imaging of the 5-HT_7 receptor. Bioorg. Med. Chem. 22 (2014) 1736–1750.

[58] J.F. Desaphy, A. Dipalma, M. De Bellis, T. Costanza, C. Gaudioso, P. Delmas, A.L. Jr. George, D.C. Camerino, Involvement of voltage-gated sodium channels blockade in the analgesic effects of orphenadrine. Pain 142 (2009) 225–235.